

IC 5063: A MERGER REMNANT WITH A HIDDEN LUMINOUS ACTIVE NUCLEUS<sup>1</sup>L. COLINA,<sup>2,3</sup> W. B. SPARKS, AND F. MACCHETTO<sup>2</sup>

Space Telescope Science Institute, 3700 San Martin Drive, Homewood Campus, Baltimore, MD 21218

*Received 1990 May 4; accepted 1990 August 31*

## ABSTRACT

Sensitive high spatial resolution optical and infrared imaging and optical spectroscopy are presented for the active galaxy IC 5063. Physical and kinematic conditions are derived for the emission regions, and deep images of the dust and optical line emission are presented. These support the proposition that the gas and dust arise from a recent merger event.

We find strong evidence for the presence of a hidden, luminous ionization source in the nucleus of IC 5063. This comprises the detection of a broad faint H $\alpha$  emission line with FWZI  $\approx$  6000 km s<sup>-1</sup>, the detection of high-excitation [Fe VII] emission lines and the presence of an extended emission-line region with a well-defined region of high excitation.

We find what is one of the best examples of a highly anisotropic ionizing radiation field, with the high-excitation line emission displaying a distinctive “X” or “conical” morphology. This cone has a 50° opening angle in projection, extends over 22 kpc and has a large-scale X-type morphology, very probably due to dust obscuration of the ionization beam. This is in turn consistent with consideration of the energetic balance between the ionized gas and infrared emission.

*Subject headings:* galaxies: individual (IC 5063) — galaxies: interactions — galaxies: nuclei

## 1. INTRODUCTION

Despite the intense theoretical and observational effort of recent years, two questions in particular remain open in the field of active galaxies. The first is whether or not a connection exists between merger events and nuclear activity, and the second is whether or not the radiation field of the nucleus is isotropic. An ideal location to study these questions in some detail is provided by the active galaxy IC 5063, PKS 2048–572, a galaxy which is known to contain high excitation extended line-emission regions, a strong, warm far-infrared excess peaking at 60  $\mu$ m, a nonthermal radio source, probably double, and a very red highly polarized nucleus in the near-infrared. The galaxy hosts properties common to both Seyfert and radio galaxies, and may represent an intermediate or transition object in this respect.

Returning to the two principal questions posed above, the first concerns the connection between interaction or merger of galaxies and the generation of starburst or nuclear activity. A large fraction of high-luminosity radio galaxies (Heckman et al. 1986; Baum et al. 1988), quasars (Hutchings 1987) and luminous *IRAS* galaxies (Sanders et al. 1988), show the presence of a companion or have peculiar optical morphology and this has been interpreted as evidence of a recent merger or interaction. Support comes also from kinematical studies of the extended emission-line regions (EELR) around powerful radio galaxies where in many cases high angular momentum, complex velocity fields without evidence of well-ordered rotation are detected (Tadhunter, Fosbury, & Quinn 1989). Also, powerful radio galaxies with strong emission lines have bluer colors relative to giant ellipticals (Smith & Heckman 1989).

In Seyfert galaxies, the evidence for a connection between

nuclear activity and interaction is less compelling (Dahari 1984; Kennicutt & Keel 1984; Bushouse 1987; MacKenty 1989), and although there are good examples of individual galaxies showing clear evidence of tidal disruptions or merger residuals (Colina et al. 1987; Fricke & Kollatschny 1989; Tadhunter & Tsvetanov 1989; Macchetto et al. 1990), there are others that do not. Also a large fraction of low-luminosity radio galaxies is associated with a system of two elliptical galaxies in interaction (Colina & Pérez-Fournon, 1990a, b). Theoretical arguments (Byrd et al. 1986, 1987; Lin, Pringle, & Rees 1988; Hernquist 1989) suggest that tidal effects produced by a close companion galaxy are effective in channeling gas deep into the nucleus of a galaxy, thereby inducing “activity.”

The second question concerns the anisotropy of the non-thermal nuclear source. Much evidence has accumulated over the last 5 years showing that all types of active galaxies could somehow radiate anisotropically (obscuration/beaming/accretion disc) and suggesting therefore that much of the diversity of AGN is simply a matter of different viewing angle (see Antonucci 1990 and Browne 1990 for reviews).

The idea that hidden, luminous, active nuclei are common received strong support with the detection by Antonucci & Miller (1985) of polarized broad emission lines in NGC 1068, a galaxy otherwise classified as Seyfert 2. This implies that there is an obscured Seyfert 1 nucleus whose radiation is seen only indirectly through scattering into our line of sight. In addition, a wide UV ionizing radiation cone has been detected in a number of other nearby Seyfert 2 galaxies (Pogge 1988a, b; Tadhunter & Tsvetanov 1989; Pérez et al. 1989; Pérez-Fournon & Wilson 1990), and alignments between radio structure and extended emission-line regions have been found both at low redshift (Unger et al. 1987; Wilson, Ward, & Haniff 1988; Wilson & Baldwin 1989; Macchetto et al. 1990) and high redshift (Chambers, Miley, & van Breugel 1987; McCarthy et al. 1987; Chambers & Miley 1989).

The galaxy IC 5063 is nearby,  $z = 0.0110$ , and is usually classified as SO. It has a number of distinctive properties,

<sup>1</sup> Based on observations collected at the European Southern Observatory and CTIO.

<sup>2</sup> Affiliated to the Astrophysics Division, ESTEC, Noordwijk, The Netherlands.

<sup>3</sup> Postal address: Fisica Teorica, Ciudad Universitaria de Canto Blanco, 28049 Madrid, Spain.

including strong extended high-excitation optical line emission, a Seyfert 2 type nucleus, powerful, warm infrared emission, extensive dust, and a double radio source (Danziger, Goss, & Wellington 1981, hereafter DGW; Bergeron, Durret, & Boksenberg 1983, hereafter BDB). An anomalously large  $M(H\ I)/L_B$  ratio has also been observed (Wardle & Knapp 1986; DGW). Although the optical characteristics are essentially “Seyfert 2,” the radio luminosity  $\log P(1.4\ \text{GHz}) = 23.8\ \text{W Hz}^{-1}$  is almost two orders of magnitude larger than the typical value for nearby Seyfert galaxies (Ulvestad & Wilson 1984), and this places IC 5063 within the low luminosity range of radio elliptical galaxies.

The optical line-emission regions extend to distances up to 19 kpc from the nucleus (BDB), lie in a disc (DGW), and present a rotational velocity field with velocity amplitude larger than measured in the stellar component (DGW; BDB). Low-resolution radio observations (FWHM  $\approx 50''$ ) with the Fleurs Synthesis Telescope show IC 5063 hosts a low-luminosity radio source with an elongation along P.A.  $270^\circ$ – $300^\circ$  (DGW). IC 5063 is also a luminous *IRAS* galaxy with  $\log L_{\text{FIR}}(L_\odot) = 10.53$  (Heckman et al. 1989). Based on its large IR polarization perpendicular to the radio axis, and its infrared spectral index, Hough et al. (1987) suggested that a blazar-type nucleus is located at the center of IC 5063.

The detection of a faint broad emission-line component (BDB; Colina et al. 1990) and the presence of an off-nuclear broad emission-line region at  $1'8$  NW of the nucleus (Wagner & Appenzeller 1989) suggest the presence of a luminous Seyfert 1 type nucleus, or perhaps more precisely a BLRG nucleus, hidden from our line of sight.

These large-scale morphological, kinematic and other characteristics therefore make IC 5063 an excellent candidate for a merger remnant and for a galaxy having a hidden luminous active nucleus. In the current work, we present new deep optical broad and narrow passband imaging, long-slit spectra along the extended emission-line regions and infrared imaging. The results provide support for the idea of a recent merger and the existence of a hidden, luminous active nucleus radiating within a relatively wide ionizing cone. In § 2 we describe the observations, and in § 3 the results including maps of the dust distribution, the ionized gas distribution and its excitation, the velocity field of the ionized gas, and the physical conditions and abundances within the ionized gas. Section 4 discusses the origin of the gas and dust, the possibility of a hidden active nucleus and the anisotropy of the ionizing radiation. Section 5 summarizes. We assume  $H_0 = 50\ \text{km s}^{-1}\ \text{Mpc}^{-1}$ , corresponding to  $1'' = 0.32\ \text{kpc}$  at the redshift of IC 5063.

## 2. OBSERVATIONS AND REDUCTIONS

### 2.1. Optical CCD Imaging and Spectroscopy

The observations are detailed in Table 1. During the 1987 August run, images using the broad-band *B*, *V*, and *R* filters and narrow band images at the redshifted [O III]  $\lambda 5007$  and  $H\alpha$  were obtained at the ESO 3.6 m telescope using the ESO Faint Object Spectrograph and Camera (EFOOSC). We also obtained spectra at two position angles, P.A.  $321^\circ$  and P.A.  $287^\circ$ , with a spectral dispersion of  $130\ \text{\AA mm}^{-1}$  and a slit width of  $2''$  projected onto the sky. The CCD detector consisted of  $516 \times 331\ 30\ \mu\text{m}$  pixels corresponding to  $0''.675\ \text{pixel}^{-1}$  on the sky. Seeing conditions were measured to be  $1''.7$ – $2''$ . The later EFOOSC observations were long-slit spectra along P.A.  $289^\circ$  using a CCD detector with  $1030 \times 660\ 15\ \mu\text{m}$  pixels, a slit

TABLE 1  
JOURNAL OF THE OBSERVATIONS OF IC 5063

Date	Instrument	Band	Exposure Time (s)	Comments
1987 Aug 26 .....	ESO 3.6 m EFOOSC	<i>B</i>	120	
		<i>B</i>	600	
		<i>V</i>	60	
		<i>V</i>	300	
		<i>R</i>	30	
		<i>R</i>	300	
		$\lambda 6627$	1800	H $\alpha$
1987 Aug 27 .....	ESO 3.6 m EFOOSC	<i>B</i>	60	
		$\lambda 5000$ – $7000$	1800	[O III]
		$\lambda 6627$	120	H $\alpha$
		$\lambda 5060$	60	[O III]
		$\lambda 5060$ – $7000$	1800	P.A. $321^\circ$
1988 May 25 .....	CTIO 1.5 m IR camera	<i>K</i>	40	P.A. $287^\circ$
		<i>H</i>	60	
1989 Oct .....	ESO 3.6 m EFOOSC	$\lambda 3600$ – $7000$	1500	P.A. $289^\circ$
		$\lambda 3600$ – $7000$	900	P.A. $289^\circ$

width  $1''$  and dispersion  $230\ \text{\AA mm}^{-1}$  to cover  $3600$ – $7000\ \text{\AA}$ . An improved seeing of  $\approx 1''$  was found during these observations.

The data were debiased and corrected for pixel-to-pixel sensitivity variations using standard techniques—the overscan region was used to estimate a constant bias level, dome flat fields were applied to the imaging data and internal quartz-halogen flat fields for the spectroscopic data. In addition, the low spectral resolution EFOOSC data were corrected for a “column offset” problem by subtracting a model of the defect (narrow stripes along the dispersion direction). The standard stars Feige 25 and LDS 749 were used for flux calibration, and standard atmospheric extinction curves were applied.

### 2.2. Infrared Imaging

The infrared images were taken with the 1.5 m telescope and IR imager at CTIO. The IR detector is described in the 1987 March NOAO Newsletter. It is a  $62 \times 58\ \text{InSb}$  array of  $75\ \mu\text{m}$  pixels with readout noise  $\approx 400$ – $500\ e^-$ , dark current  $\approx 200\ e^- s^{-1}$  and resolution  $0''.92\ \text{pixel}^{-1}$ . IC 5063 was observed on the night of 1988 May 25, using *J*, *H* and *K* filters, centered at 1.24, 1.65, and  $2.16\ \mu\text{m}$  and having bandwidth 0.30, 0.27 and  $0.38\ \mu\text{m}$ , respectively.

The observational techniques appropriate for infrared arrays differ somewhat from those of CCDs, the major problem being the sky brightness. To cope with this, we repeatedly observed the object and regions of sky at distances  $\approx 3'$  from it, and combined these as described below; five for the galaxy and two for the sky for the *K* filter (exposure time = 40 s); one for the sky and three for the galaxy for the *H* and *J* filters (exposure times = 60 s). The data were first debiased by subtracting a master bias image appropriate to that night. The detector was found to show a 2.2% nonlinearity at  $10^4$  counts. The linearization correction was determined to  $\approx 3\%$  accuracy from flat-field observations of different duration, and this correction was then applied to the debiased data. The “sky” frames around the object were combined to create a single sky image per filter (incorporating any residual dark count and medium time scale bias fluctuations) which was then subtracted from each of the data frames. The master sky frame was the pixel-by-pixel median of the individual sky frames. Bad



### 3.2. The Infrared Nucleus and Surface Brightness

Axon, Bailey, & Hough (1982) reported the discovery of an extremely red infrared nucleus in IC 5063, which was subsequently found to have a very high polarization  $\approx 17\%$  (Hough et al. 1987). We can use our infrared imaging to remeasure the flux of the nucleus and check for variability and to investigate the radial surface brightness profile of the stars.

To calibrate the images, in order to correct for time-varying sky brightness we adjusted the background level of the  $H$  and  $K$  images slightly to (conservatively) minimize infrared color gradients across the range  $\approx 10''$ – $20''$ , and then took average zero points by comparing simulated aperture photometry from the images to the photometry of Axon et al. (1982) (their two outermost measurements). Surface brightness profiles with ellipticity  $10(1 - b/a) = 2.0$  in P.A.  $300^\circ$  were then derived. The galaxy is quite well-described by an  $R^{1/4}$  law, with  $\mu_J = 3.829R^{1/4} + 11.54$ , as in Figure 2, and with no evidence of a bright nucleus at  $J$ . This indicates a classification of IC 5063 as a very early-type S0 or elliptical galaxy. To estimate nuclear magnitudes, the  $J$  image was linearly scaled to match the  $H$  and  $K$  images in the region  $5''$ – $20''$ , and then subtracted. The magnitude of the remaining (nuclear) emission was then measured to be  $K = 12.88$  and  $H \approx 14.91$ , possibly somewhat fainter. This compares extremely well with the  $K$ -magnitude of 12.89 inferred by Hough et al. (1987) and the corresponding spectral index is 4.5 or greater, compared to a previously determined 4.6. We therefore find no evidence for variability and confirm previous estimates of the luminosity and extreme spectral index of the nucleus. Figure 3 illustrates this with the corresponding  $J - K$  surface brightness profile.

### 3.3. Gas and Dust Distribution

#### 3.3.1. Dust Lane Distribution and Associated Gas Mass

Figure 4a (Plate 1) shows the direct  $V$  300 s frame. Dust lanes are clearly visible to the north of the nucleus. To map and quantify this distribution of dust within the galaxy, ellipses were fitted to the  $R$  images, and models having purely elliptical isophotes were generated from these isophotal profiles. The  $V$  images were then divided by these models of the underlying

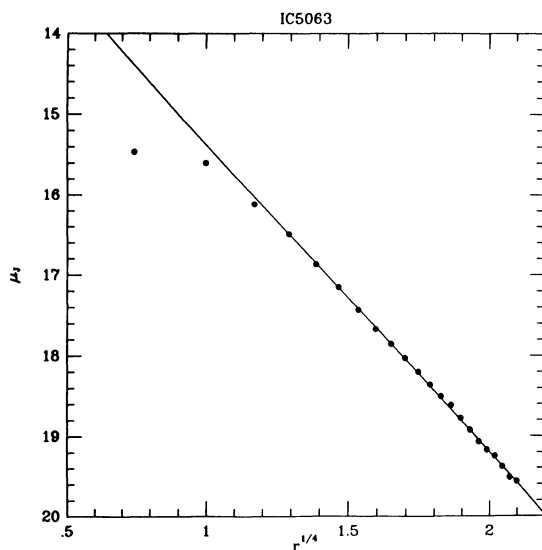


FIG. 2.—Surface brightness profile of IC 5063 in the  $J$  band. Superposed is a de Vaucouleurs  $r^{1/4}$ -law with slope of 3.829 and zero point of 11.54.

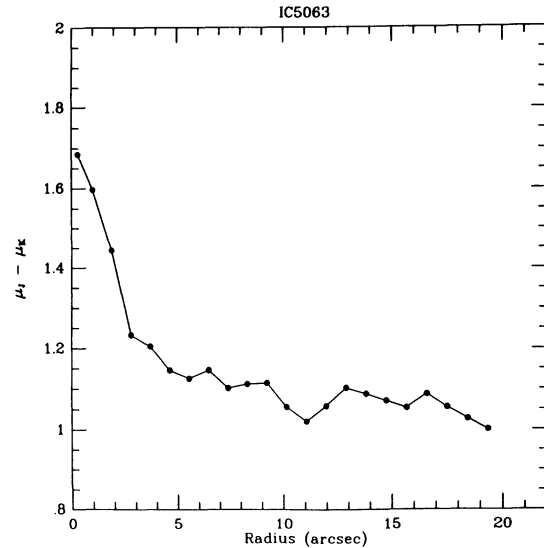


FIG. 3.— $J - K$  color as a function of radius from the infrared images. Notice the nucleus is 0.5 mag redder than the rest of the galaxy.

stellar light distribution (see Sparks et al. 1985). The result is an image of the optical depth at  $V$  or equivalently a map of  $A_V$ . Figure 4b (Plate 2) shows the result of dividing the 300 s  $V$  frame by such a model. The gray scale runs from the background (shown as gray) of no obvious extinction to white, corresponding to an  $A_V \approx 0.3$  mag. Typical values within the dust complex are  $A_V \sim 0.2$ – $0.4$  mag. For a normal gas-to-dust ratio, this corresponds to  $4$ – $8 \times 10^{20}$  atoms  $\text{cm}^{-2}$  column density of associated hydrogen. The actual column density may be higher since heavy element abundances are low (below), and hence the dust-to-gas ratio may be also low.

The dust map, Figure 4b, shows a complex system of dust lanes mostly concentrated in the northern side of IC 5063. The morphology represents a zig-zagging distribution running approximately parallel to the major axis of IC 5063 and going all the way down into the nucleus. These dust lanes are not only concentrated in the central regions but extend as far as the data permit observation beyond the main stellar body of the galaxy (see Fig. 4b), and they possess a relatively weak symmetry with respect to the main body of the galaxy. The most symmetric dust lanes are located nearest the nucleus. This supports the idea that the dust has an external origin, since such structures are unlikely to survive many dynamical time scales due to differential precession effects, and they may well be in the process of settling into the plane of the galaxy.

The total amount of gas corresponding to the observed extinction for a normal gas-to-dust ratio is  $\approx 4 \times 10^8 M_\odot$ , assuming symmetry on the far side of the galaxy in the form of dust which is not seen in absorption.

#### 3.3.2. Ionized Gas Distribution

The overall distribution of ionized gas is presented in Figure 5a and 5b (Plates 3 and 4) ( $H\alpha$  and  $[\text{O III}] \lambda 5007$  light distribution). The morphology is that of a cylindrical or elliptical main body also having three radial filaments along positions P.A.  $285^\circ$ – $290^\circ$ , P.A.  $310^\circ$ – $315^\circ$  and P.A.  $325^\circ$ – $330^\circ$ . Therefore, the basic symmetry axis of these extended emission line regions lies along the major axis of the light distribution (P.A.  $303^\circ \pm 5^\circ$ ; DGW). The size of the emission-line regions corresponds to  $69''$  by  $20''$  (i.e., 22 by 6.4 kpc) along their major and minor axis, respectively.



FIG. 4a

FIG. 4.—(a) Direct 300 s  $V$  image of IC 5063 clearly showing the presence of dust-lanes in the northern half of the galaxy. North is at the top and east is to the left. The field of view is  $169'' \times 155''$ . (b)  $V - \text{Model } R$  ratio image showing the dust optical depth throughout the galaxy. Notice the curious zig-zagging morphology of the system of dust lanes located in the northern side of IC 5063.

COLINA, SPARKS, & MACCHETTO (see 370, 105)

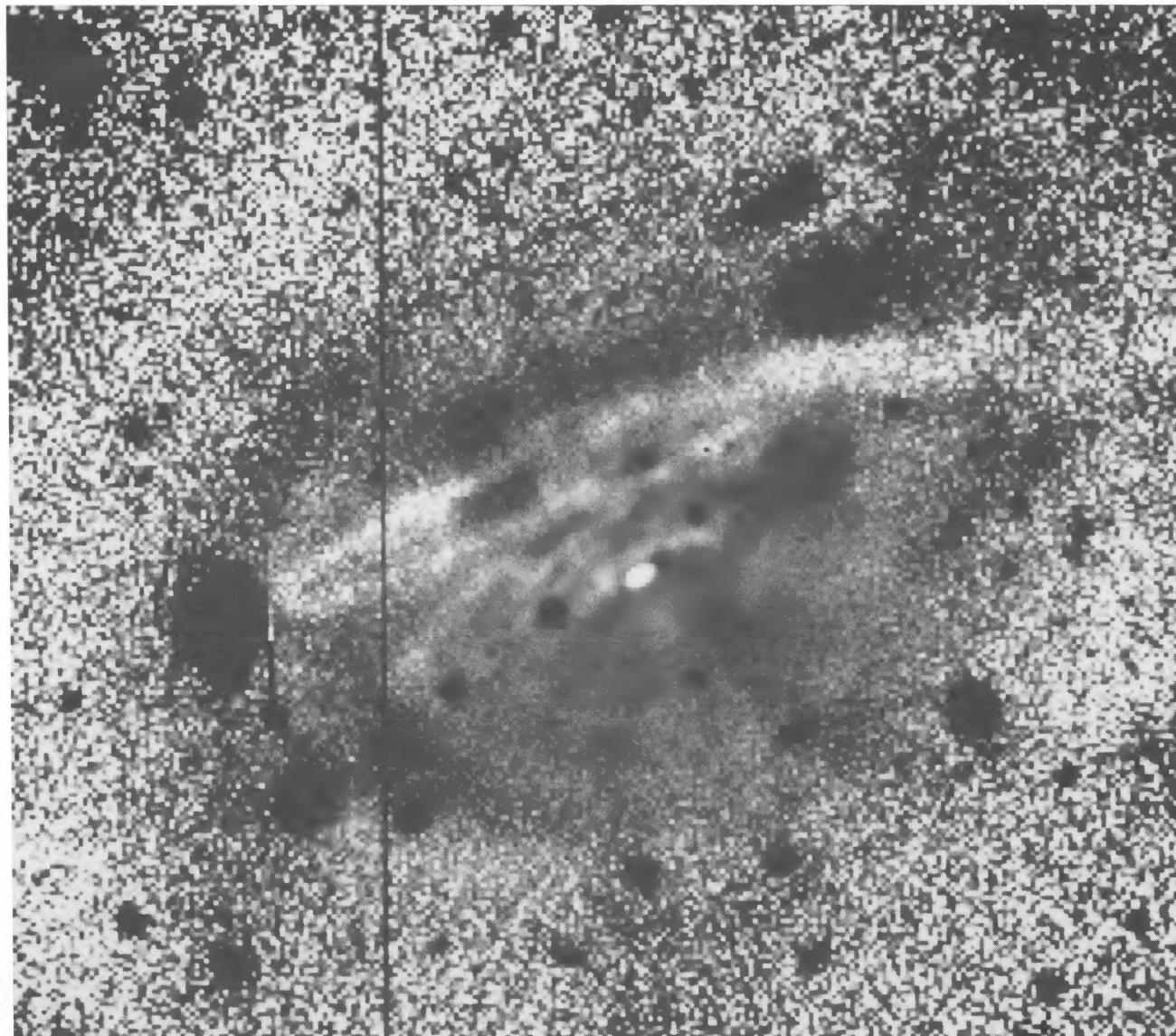


FIG. 4b

COLINA, SPARKS, & MACCHETTO (see 370, 105)

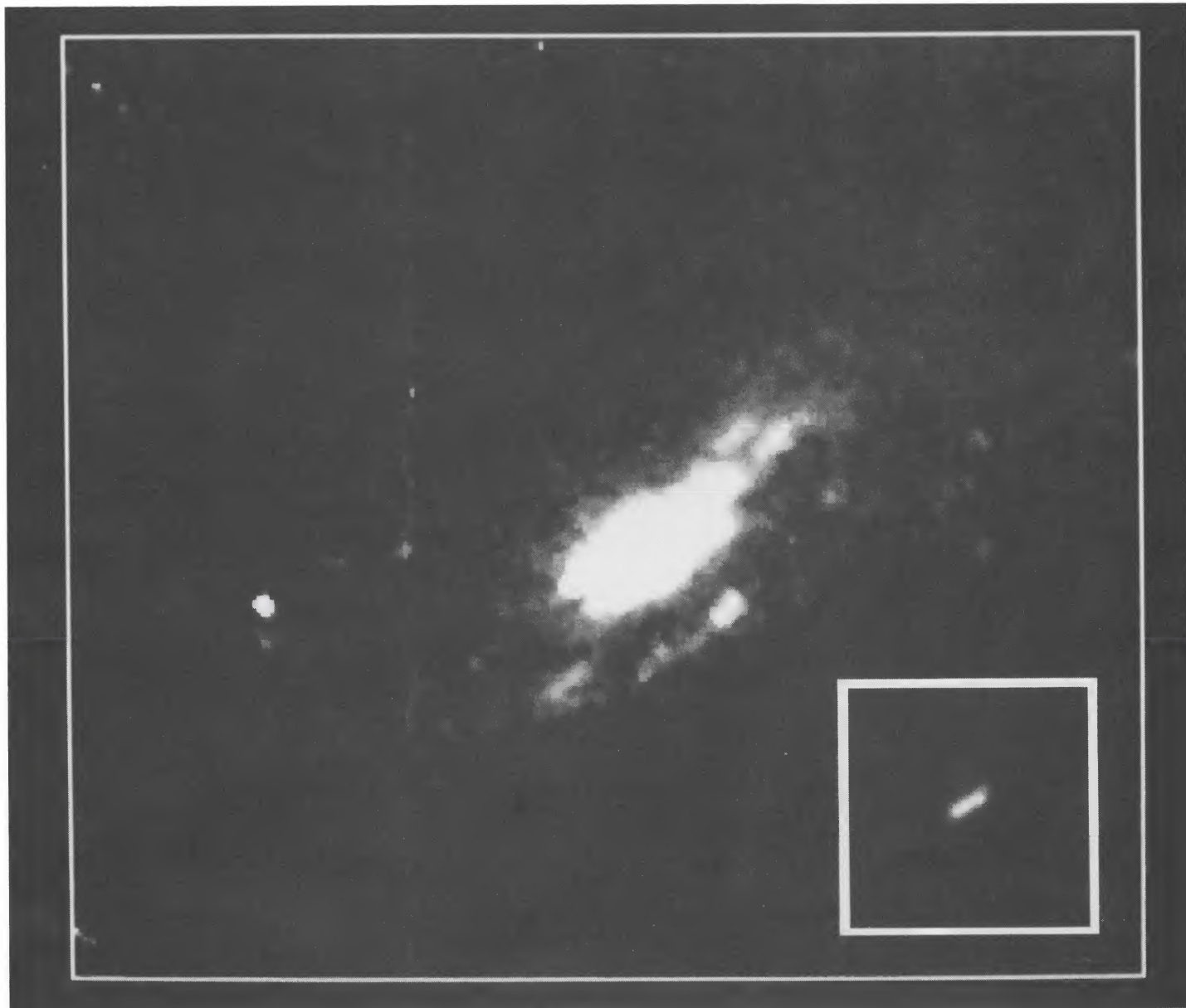


FIG. 5a

FIG. 5.—(a) Image of IC 5063 showing the extended emission-line regions in the  $H\alpha$  line. The orientation and field of view is the same as Fig. 4. (b) Same as previous figure, but with  $[O III] \lambda 5007$ . The total size of these regions is  $69'' \times 20''$  corresponding to  $22 \times 6.4$  kpc. The insets show the nuclear regions.

COLINA, SPARKS, & MACCHETTO (see 370, 105)

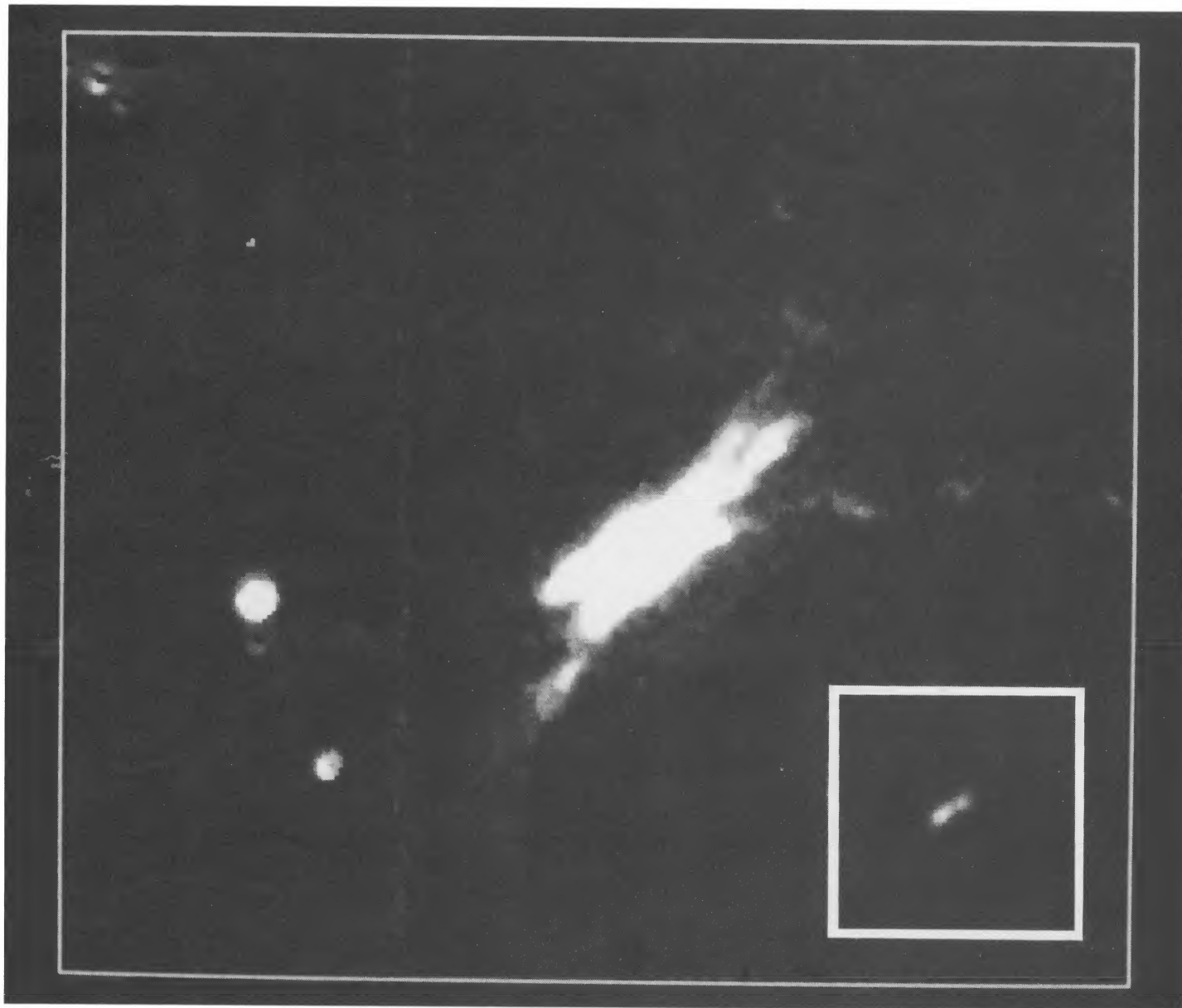


FIG. 5b

COLINA, SPARKS, & MACCHETTO (see 370, 105)

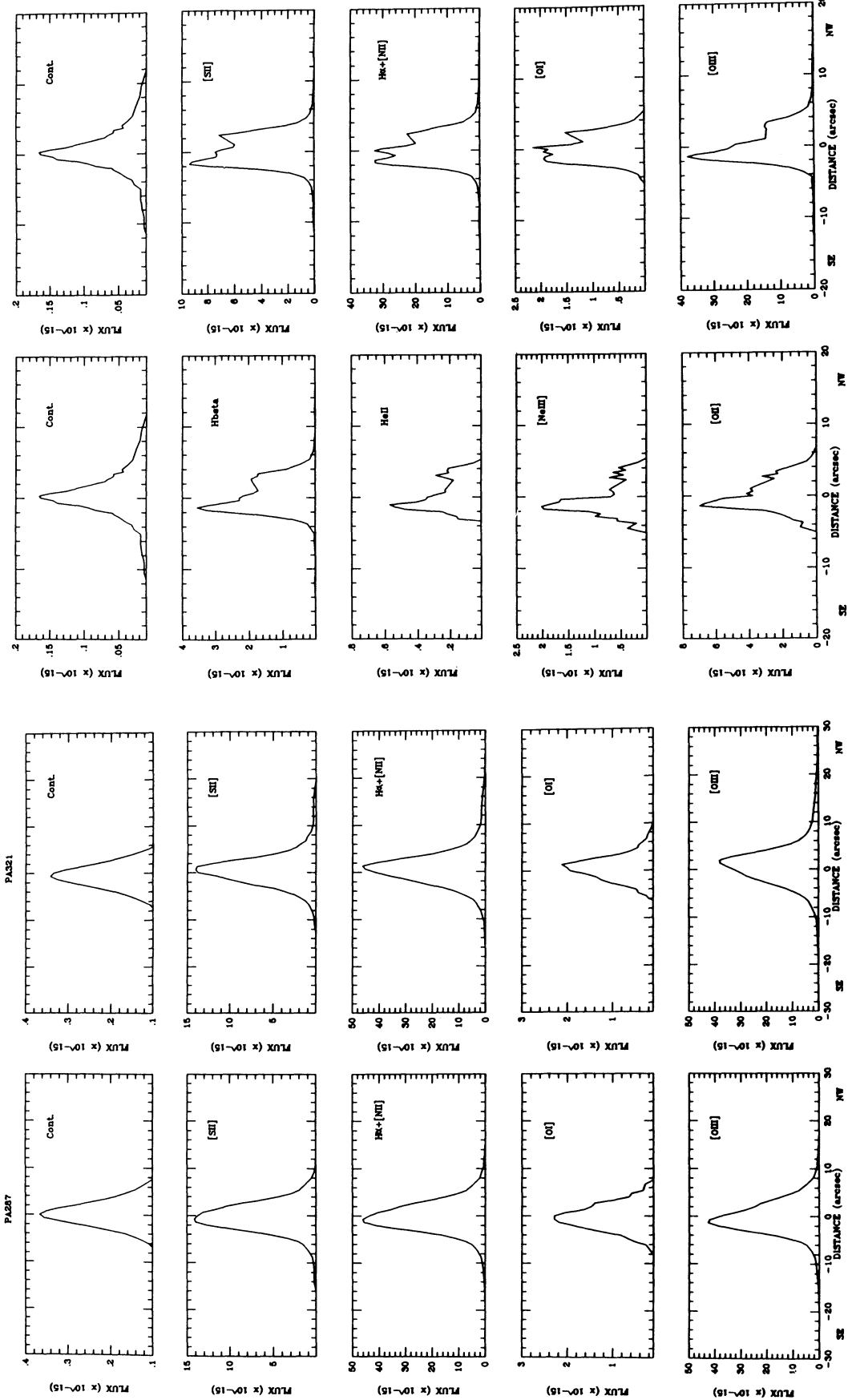


FIG. 6.—(a) Radial distribution of the continuum and main emission lines [O III]  $\lambda$ 5007, [O I]  $\lambda$ 8446, H $\alpha$  + [N II]  $\lambda$ 6300, H $\beta$  + [N II]  $\lambda$ 6584, and [S II]  $\lambda$ 46717, 6731 along position angles P.A. 287° and P.A. 321°. The flux is in units of  $10^{-15}$  ergs  $\text{cm}^{-2}$   $\text{s}^{-1}$ . The offsets of emission-line intensity peak with respect to that of the continuum are clearly visible. (b) Same as the previous figure, but along position angle P.A. 289°. Here, we also show the [O II]  $\lambda$ 3727, [Ne III]  $\lambda$ 3869, He II  $\lambda$ 4686, and H $\beta$  emission lines.

It is also important to remark that the high-excitation gas, traced by the [O III] distribution, is more concentrated along the major axis while the low-excitation gas, traced by the H $\alpha$  distribution extends further along the minor axis giving a “rounder” geometry. This is even more clear in the excitation map (see § 4.2 and Fig. 14).

Also a faint extension of the P.A. 285° filament is detected in [O III] bending to the west at P.A. 270° and at distances up to 90″ from the nucleus (i.e., 29 kpc). This extension is oriented along the direction of a second faint radio source located along P.A. 276° at a distance of 161″ from IC 5063 (DGW). It is not yet clear if these two phenomena have any physical connection. The H $\alpha$  emission, on the other hand, shows a SW filament which ends in a bright emission knot. This is extremely similar to the *dust* morphology on the *northern* side of the galaxy, and may be due to illumination of optically thick material by a central ionizing source.

The radial distribution of the main emission lines along the different position angles are presented in Figures 6a and 6b, as derived from our long-slit spectroscopy. In these figures the  $x$  coordinate represents the distance in the plane of the sky, while the  $y$  coordinate indicates the flux in units of  $10^{-15}$  ergs  $s^{-1}$   $cm^{-2}$ . It is noticeable that the emission peak of *all* the emission lines is *displaced with respect to the nucleus* defined as the position where the continuum has its maximum. Along P.A. 287° and P.A. 289° the emission-line distribution peaks 1.5–2″ SE of the nucleus, while at P.A. 321° it peaks at 2″ NW of the nucleus. These peaks are marginally resolved with the present imaging resolution (Fig. 5b) and are confirmed in higher resolution unpublished [O III] images. A distinct kinematical behavior appears to exist in these regions (see next section).

### 3.4. The Velocity Field of the Ionized Gas

The velocity field along the different position angles was obtained by measuring the centroid of the H $\alpha$ , [N II]  $\lambda$ 6584

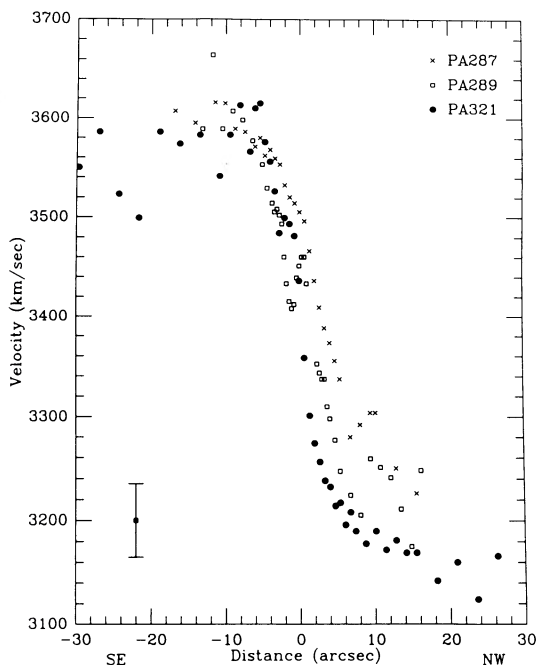


FIG. 7.—Measured velocity field along the different position angles. The deep reverse velocity feature at around 1.5 SE to the nucleus at position angle P.A. 289° is clearly detected.

and [S II]  $\lambda$ 6717, 6731 emission lines. Figure 7 represents observed velocity as a function of distance on the plane of the sky for the different orientations. Assuming an inclination of 55° to the line of sight and a position angle of the major axis around 120°–123° (DGW), the distances in the plane of the sky can be transformed into distances in the plane of the galaxy multiplying by factors 1.09, 1.07, and 1.06 for P.A. 321°, P.A. 287°, and P.A. 289°, respectively.

The uncertainty in velocity determination was estimated by the dispersion of the wavelength measurements of the strong [O I]  $\lambda$ 5577, 6300 sky emission lines. This corresponds to  $\pm 35$  km  $s^{-1}$  (or  $\pm 0.75$  Å) and is similar to the uncertainty obtained comparing the velocity of the IC 5063 nucleus obtained in the three different slit positions ( $\pm 36$  km  $s^{-1}$ ). This uncertainty increases up to 60 km  $s^{-1}$  or more at large distances ( $\geq 15''$ ) where the signal-to-noise ratio of the emission lines decreases very rapidly.

As already detected by DGW and BDB the observed velocity field along the different position angles, shows a clear rotational pattern with steep velocity gradients within the first 8″ around the nucleus and a flatter velocity profile elsewhere up to distances of 20″–25″ (i.e., 6.4–8 kpc). The total velocity amplitude between the two sides of the galaxy corresponds to  $\approx 400$  km  $s^{-1}$  and the steepest gradients (by a small amount) are found along P.A. 321°. These characteristics agree with the idea that the emission-line gas basically lies in a disc with dynamical major axis at P.A.  $300^\circ \pm 3^\circ$  (DGW) which also corresponds to the major axis of the light distribution (P.A.  $303^\circ \pm 5^\circ$ , DGW). The total mass of the galaxy within a radius of 19 kpc corresponds to  $3.1 \times 10^{11} M_\odot$  as derived from ionized gas rotation curves (BDB).

At around 1.4 SE of the nucleus at P.A. 289° in the data obtained in good seeing, we find a feature in the velocity curve such that at this location the velocity is about  $-80$  km  $s^{-1}$  from the expected rotational curve value. This confirms the detection by Caldwell & Phillips (1981) of an independent emission-line component with a large negative velocity at 2.5 SE of the nucleus at P.A. 300° and adds evidence to support the recently reported “counter-rotating” gas detected in the central 2″ of the nucleus along P.A. 305° (Wagner & Appenzeller 1989). If this velocity structure is indeed due to gas-counter-rotating with respect to the stars and outer gas regions, such gas must have a large inclination with respect to the plane of the sky and must rotate very rapidly in order to permit detection against the steeply increasing underlying rotational gradients. An alternative explanation for the phenomenon may be radial gaseous flows, possibly associated with scattering. In any event, it seems that the dynamical properties of the gas around 2″ of the nucleus are independent of those at larger distances. This feature is not seen in the other two position angles, probably due to the combined effects of lower spectral resolution and inferior seeing conditions (see § 2.1 for details).

### 3.5. Extinction within the Emission-Line Regions

We can get a direct estimate of the extinction within the emission-line regions using the Balmer line H $\alpha$ /H $\beta$  and H $\beta$ /H $\gamma$  ratios along the direction P.A. 289°. The extinction from the H $\alpha$ /H $\beta$  ratio is systematically larger than from the H $\beta$ /H $\gamma$  ratio, as already noted for the nucleus alone by BDB [mean  $E(B-V) = 0.61$  vs.  $E(B-V) = 0.21$ ]. The H $\alpha$  line flux is affected however by the presence of a faint broad component in the nuclear regions (see § 4.2), while the blend with the bright

[N II]  $\lambda\lambda$  6548, 6583 emission lines adds another uncertainty to the measured flux. It therefore seems that the  $H\alpha/H\beta$  ratio cannot be considered a very reliable reddening indicator, although it has been recognized that narrow-line radio galaxies appear to have larger  $H\alpha/H\beta$  ratios than that expected from pure case B recombination (Koski 1978; Ferland & Osterbrock 1985), and this has been interpreted as evidence of the existence of dust within the emission-line regions.

On the other hand,  $H\gamma$  at a wavelength  $\lambda$ 4340, is slightly blended with the [O III]  $\lambda$ 4363 emission line. However the effect of the blending is not as critical as in the case of  $H\alpha$  and amounts to an uncertainty of  $\approx 10\%$  of the flux of the emission line. Assuming an error of 5% in the  $H\beta$  flux, the uncertainty in the  $H\beta/H\gamma$  ratio (0.12 times the ratio itself) translates into an uncertainty of  $E(B-V) = \pm 0.26$ .

Subject to these uncertainties and considering the  $H\gamma/H\beta$  ratio (Fig. 8a) as the best reddening indicator, we deduce that the extended emission-line regions located to the SE of the nucleus (the side which is receding from us) are consistent with extinction equal to zero, while the regions located toward the NW (the side which is approaching us) have a mean extinction of around  $E(B-V) = 0.40$  at distances  $2''-4''$  from the nucleus (see Fig. 8b for details). The image of the dust found  $A_V \approx 0.3$  in the dust-lanes farther out in the galaxy. That estimate is a lower limit to the true extinction since seeing and nonunity covering factor both act to reduce the apparent extinction, and it seems reasonable to associate the reddening of the emission-line spectrum with an inwards extrapolation of the dust seen at large radii elsewhere in the galaxy.

Finally, the continuum light distribution is reasonably symmetric near the nucleus, and its peak lies close to the center of ellipses fitted at larger radii. This argues against the presence of

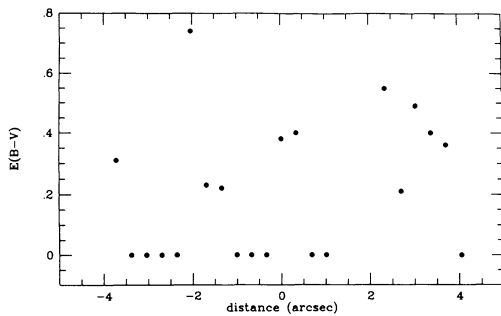


FIG. 8a

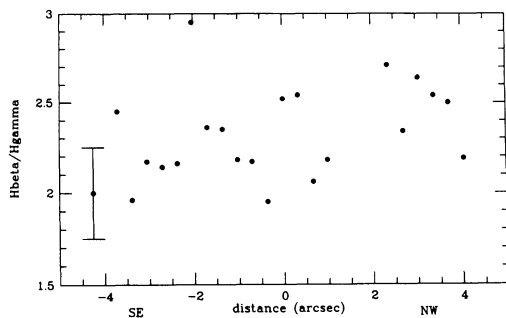


FIG. 8b

FIG. 8.—(a) Observed  $H\gamma/H\beta$  ratio as a function of radius for P.A.  $289^\circ$ . (b) Extinction values  $E(B-V)$  as obtained from the previous  $H\gamma/H\beta$  measurements. The uncertainties in the extinction measurements correspond to  $\pm 0.26$ .

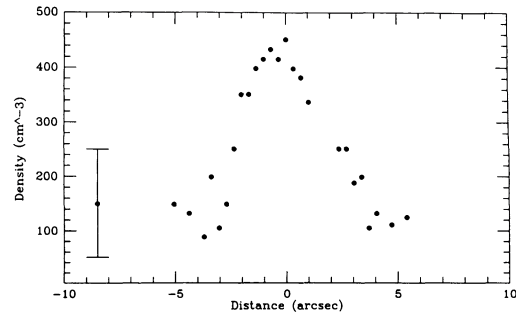


FIG. 9a

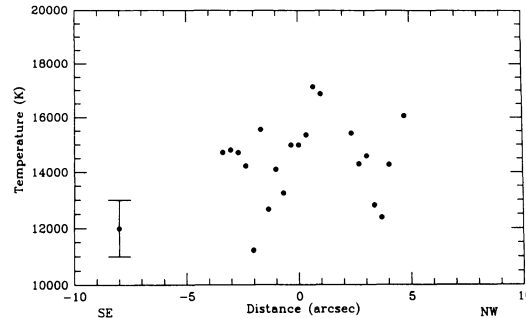


FIG. 9b

FIG. 9.—(a) Measured density gradient as obtained from the [S II]  $\lambda$ 6717/ $\lambda$ 6731 line ratio along position P.A.  $289^\circ$ . (b) Measured temperature values as obtained from the [O III] ( $\lambda$ 4959 + 5007)/ $\lambda$ 4363 emission-line ratio along P.A.  $289^\circ$ .

very large amounts of dust in the nuclear region, unless such dust was very centrally concentrated.

### 3.6. Physical Conditions in the Ionized Gas

#### 3.6.1. Electron Density

The electron density was measured as a function of radius using the [S II]  $\lambda$ 6717/[S II]  $\lambda$ 6731 line ratio (see Aller 1984). The results obtained along the position angle P.A.  $289^\circ$  are presented in Figure 9a. Although the uncertainties in the density determination are of the order of  $100 \text{ cm}^{-3}$ , a steep gradient in the density is clearly visible, varying from  $N_e = 400-450 \text{ cm}^{-3}$  in the nucleus to  $N_e = 100 \text{ cm}^{-3}$  at distances of  $5''$  from the nucleus. Beyond these distances the [S II] line ratio enters the low-density regime (i.e.,  $N_e \leq 100 \text{ cm}^{-3}$ ), and the signal-to-noise ratio decreases rapidly making density measurement uncertain. Our results at these larger distances indicate that the density is below  $100 \text{ cm}^{-3}$ . If we parameterize the density gradient as  $N_e \propto r^{-\beta}$ , the data are consistent with a slope  $\beta = 0.6$ , although somewhat steeper gradients cannot be ruled out.

The density estimates from the other two position angles show similar behavior but with more scatter due most likely to a combination of lower spectral resolution and worse seeing conditions. Such effects dilute spatial differences and make the results of deblending less reliable. Nevertheless, for these positions angles we measured mean density values of  $N_e = 180 \pm 76 \text{ cm}^{-3}$  and  $N_e = 244 \pm 54 \text{ cm}^{-3}$  within  $7''$  of the nucleus and along position angles P.A.  $321^\circ$  and P.A.  $287^\circ$ , respectively.

#### 3.6.2. Electron Temperature

The electron temperature has been measured along P.A.  $289^\circ$  using the [O III]  $\lambda\lambda$ 4959, 5007/ $\lambda$ 4363 emission-line ratio.

Following Aller (1984), for density in the range 100–400 cm<sup>-3</sup>, the temperature is

$$T_e = 14,320 \left[ \log \frac{F([\text{O III}] \lambda\lambda 4959, 5007)}{F([\text{O III}] \lambda 4363)} - 0.8865 \right]^{-1} \text{ K} . \quad (1)$$

The temperatures obtained in this way are presented in Figure 9b as a function of distance along P.A. 289°. The mean value within 5" of the nucleus corresponds to  $T_e = 14321 \pm 1243$  K, in agreement with BDB for the nucleus.

### 3.7. Abundances in the Ionized Gas

We can estimate the abundance of oxygen in the emission-line gas using the [O III]  $\lambda\lambda 4959, 5007$  and [O II]  $\lambda 3727$  intensities. Again, following Aller (1984), for temperature  $T_e \approx 15,000$  K and densities in the range  $N_e = 100$ –500 cm<sup>-3</sup>:

$$\frac{\text{O}}{\text{H}} \approx \frac{(\text{O}^{++} + \text{O}^+)}{\text{H}^+} = 8.24 \times 10^{-6} \frac{I([\text{O III}])}{I(\text{H}\beta)} + 2.632 \times 10^{-9} L_j(x, 1.5) \frac{I([\text{O II}])}{I(\text{H}\beta)}, \quad (2)$$

where  $L_j(x, 1.5)$  ranges from 3300 to 3600, and  $x = 0.01N_e/\sqrt{T}$ . We obtain a value O/H of  $2.4 \times 10^{-4}$  which is a factor around 3 *under* solar abundances. This result is in agreement with measurements of BDB, who found underabundances of 2.5, 5.5, and 10 times solar at the nucleus, 2 and 6 kpc from it.

### 3.8. The Amount of Ionized Gas

The amount and filling factor of the ionized gas can be obtained using the luminosity measured in the Balmer lines H $\alpha$ , H $\beta$ , or in collisionally excited lines like [O III]  $\lambda 5007$ . The amount of gas is given by  $M_g = (N_p m_p + N_{\text{He}} m_{\text{He}}) L(\text{line}) \epsilon^{-1}(\text{line})$  where  $L(\text{line})$  is the luminosity in the line,  $N_{\text{He}} = 0.1N_p = 0.1N_e$  and  $\epsilon(\text{line})$  is the emissivity in the line given by  $\epsilon(\text{H}\alpha) = 2.65 \times 10^{-25} N_e^2 \text{ ergs s}^{-1} \text{ cm}^{-3}$ ,  $\epsilon(\text{H}\beta) = 9.45 \times 10^{-26} N_e^2 \text{ ergs s}^{-1} \text{ cm}^{-3}$ , and  $\epsilon([\text{O III}] \lambda 5007) = 7.74 \times 10^{-21} N(\text{O}^{++}) N_e \text{ ergs s}^{-1} \text{ cm}^{-3}$ . Therefore, the amount of ionized gas can be expressed as a function of the line luminosity (in ergs s<sup>-1</sup>) and the gas electron density (in cm<sup>-3</sup>) as follows:

$$M_g = \begin{cases} 4.44 \times 10^{-33} L(\text{H}\alpha) \times N_e^{-1} M_\odot , \\ 1.24 \times 10^{-32} L(\text{H}\beta) \times N_e^{-1} M_\odot , \\ 1.21 \times 10^{-33} L([\text{O III}] 5007) \times N_e^{-1} M_\odot . \end{cases} \quad (3)$$

Assuming a mean density of  $N_e = 200$ –250 cm<sup>-3</sup> and given

the total luminosity of the H $\alpha$ , H $\beta$ , and [O III]  $\lambda 5007$  lines equal to  $1.4 \times 10^{41}$ ,  $2.48 \times 10^{40}$ , and  $2.41 \times 10^{41}$  ergs s<sup>-1</sup> over a region of 4.0 by 0.3 kpc in size along P.A. 289°, a total mass in the range  $1$ – $3.5 \times 10^6 M_\odot$  is obtained.

The total H $\alpha$  and [O III]  $\lambda 5007$  and luminosities measured from our images correspond to  $\log L(\text{H}\alpha) = 41.52$  ergs s<sup>-1</sup> and  $\log L([\text{O III}] \lambda 5007) = 41.82$  ergs s<sup>-1</sup>, the total mass will be in the range  $4$ – $8 \times 10^6 M_\odot$  if the density in the outer emission-line regions is also  $N_e = 200$  cm<sup>-3</sup>. Since our data (see § 3.6.1) show a steep decrease in the density outwards, this value should be considered as a lower limit to the total mass of ionized gas present in these regions.

Given a density and assuming that the volume of the emission-line regions is  $V = l^{1.5} a^{1.5}$  where  $l$  and  $a$  are the projected length and width of the emitting regions, the filling factor ( $f$ ) can be obtained from the expression

$$f = L(\text{line}) \times \epsilon^{-1}(\text{line}) \times l^{-1.5} \times a^{-1.5} . \quad (4)$$

Equations (7), (8), and (9) may be combined to derive:

$$f = \begin{cases} 1.27 \times 10^{-40} L(\text{H}\alpha) \times N_e^{-2} \times l^{-1.5} \times a^{-1.5} , \\ 3.55 \times 10^{-40} L(\text{H}\beta) \times N_e^{-2} \times l^{-1.5} \times a^{-1.5} , \\ 3.47 \times 10^{-41} L([\text{O III}] 5007) \times N_e^{-2} \times l^{-1.5} \times a^{-1.5} , \end{cases} \quad (5)$$

where  $l$  and  $a$  are in kpc. For the line luminosities and densities given above, we obtain a filling factor  $f \approx 10^{-4}$  for the inner regions (distances up to 2 kpc from the nucleus).

### 3.9. Excitation Conditions in the Ionized Gas

The line ratios of the stronger emission lines are presented in Figures 10a and 10b as a function of distance for the various position angles. These ratios have been obtained from observed fluxes, and no internal reddening correction has been applied.

In order to get the excitation conditions in the extended emission-line regions, we compare the different emission-line ratios with the diagnostic diagrams as presented in Robinson et al. (1987). The mean values for these line ratios for the NW, SE regions and nucleus at the different position angles are presented in Table 3. These ratios are consistent with an ionization parameter  $U = 7 \times 10^{-4}$ – $8 \times 10^{-4}$  ( $U = L_{\text{ion}} \times (4\pi)^{-1} \times R^{-2} \times N_e^{-1} \times c^{-1}$ ) from a  $T = 1.3 \times 10^5$  K ionizing blackbody spectrum—a value which agrees well with those found in extended emission-line regions (EELR) around powerful radio galaxies (Robinson et al. 1987). On the other hand, if one tries to fit the observed line ratios with a non-thermal power-law ionization source, the [N II]/H $\alpha$  is higher

TABLE 3  
MEAN EMISSION-LINE INTENSITY RATIOS IN IC 5063

Region	[O I]6300/[O III]5007	[N II]6584/H $\alpha$	[S II]6725/H $\alpha$	[O I]6300/H $\alpha$	Distance (kpc)
NW P.A. 321°	-1.40 ± 0.10	-0.23 ± 0.02	-0.30 ± 0.06	-1.12 ± 0.08	1.54
Nucleus	-1.25 ± 0.02	-0.17 ± 0.01	-0.28 ± 0.01	-1.06 ± 0.02	...
SE P.A. 231°	-1.37 ± 0.07	-0.16 ± 0.01	-0.29 ± 0.03	-1.06 ± 0.04	1.30
NW P.A. 287°	-1.28 ± 0.07	-0.17 ± 0.01	-0.30 ± 0.03	-1.02 ± 0.06	1.28
Nucleus	-1.23 ± 0.03	-0.17 ± 0.01	-0.28 ± 0.02	-1.00 ± 0.02	...
SE P.A. 287°	-1.26 ± 0.06	-0.17 ± 0.01	-0.31 ± 0.03	-0.99 ± 0.07	1.28
Nucleus	-1.09 ± 0.05	-0.28 ± 0.02	-0.29 ± 0.04	-0.95 ± 0.06	...
SE P.A. 289°	-1.29 ± 0.05	-0.17 ± 0.01	-0.30 ± 0.02	-0.96 ± 0.03	0.70

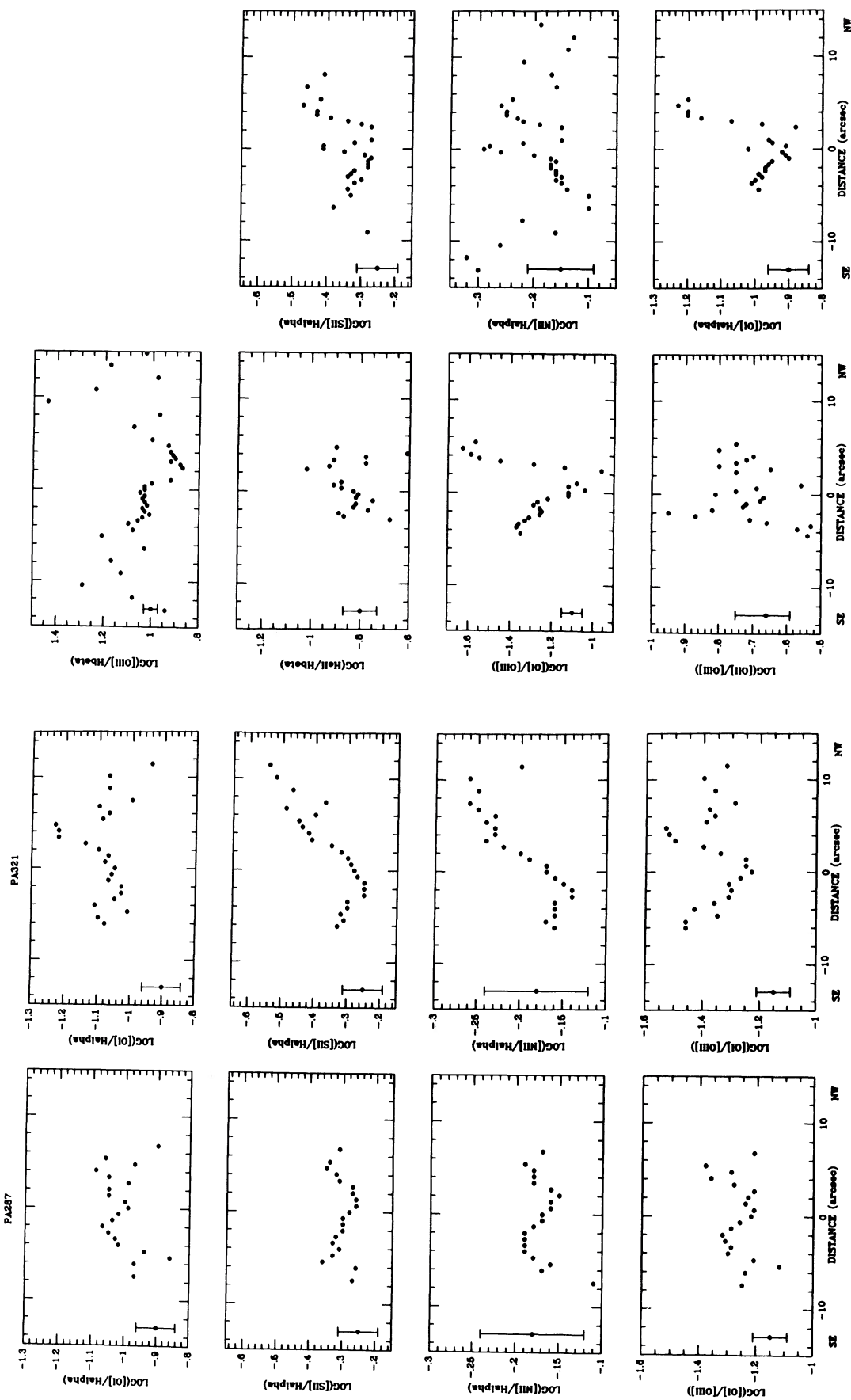


FIG. 10a

FIG. 10b

FIG. 10.—(a) Radial distribution of the main emission-line ratios along P.A. 287° and P.A. 321°. The emission lines correspond to those represented in Fig. 6. Positive excitation gradients are clearly visible to the NW. The error bar indicates the mean uncertainty in the inner 10" from the nucleus, while beyond that distance the scatter indicates the uncertainty in the measurements. (b) Same as the previous figure, but along P.A. 289°.

than predicted. The remainder of the strong-line ratios could be obtained with such a power-law continuum ( $\alpha = 1.5$  where  $F_\nu \propto \nu^{-\alpha}$ ) although with an ionization parameter 20 times larger, i.e., 20 times more ionizing photons than required by a blackbody spectrum.

Another important result obtained from these diagrams is the detection of positive excitation gradients outwards from the nucleus. This is most clearly visible in the  $[\text{O I}] \lambda 6300/[\text{O III}] \lambda 5007$  ratio along to the NW at positions P.A.  $289^\circ$  and P.A.  $321^\circ$ . This effect is also seen when looking at the ratios of the low excitation lines  $[\text{O I}] \lambda 6300$ ,  $[\text{S II}] \lambda 6725$  and  $[\text{N II}] \lambda 6584$  versus  $\text{H}\alpha$ . Positive excitation gradients were also found by BDB along a different position angle (P.A.  $310^\circ$ ). Also the extended emission-line regions around other radio galaxies often show an ionization parameter larger than in the nucleus of the galaxy itself (Robinson et al. 1987), a result which is not fully understood.

We now consider four possible effects to explain this: (1) differential extinction, (2) abundance/temperature gradients, (3) density gradients and, (4) a local ionization source.

### 3.9.1. Differential Extinction Effects

It is very unlikely that differential extinction effects are important in modifying the line ratios since excitation gradients are also seen in the ratios of  $[\text{N II}] \lambda 6584/\text{H}\alpha$  and  $[\text{S II}] \lambda 6725/\text{H}\alpha$  which are almost completely unaffected by extinction. Also, extinction would *increase* the  $[\text{O I}]/[\text{O III}]$  ratio, contrary to the observations. Finally, the extinction obtained from  $\text{H}\gamma/\text{H}\beta$  gives a maximum value of  $A_V \approx 1.2$  magnitudes without any evidence of a systematic radial increase towards the outer regions along P.A.  $289^\circ$ . We therefore conclude that dust extinction effects are very unlikely to cause the observed trend.

### 3.9.2. Abundance Gradient Effects

BDB measured a steep positive temperature gradient and negative abundance gradient over the first  $18''$  (i.e., 6 kpc)

around the nucleus, as described above. We measure the abundances within the first 2 kpc along position angles P.A.  $289^\circ$  (see § 3.6) and find values consistent with those of BDB. Although decreasing heavy element abundance could be important in explaining the  $[\text{N II}]/\text{H}\alpha$  and  $[\text{S II}]/\text{H}\alpha$  negative gradients, this alone cannot explain the gradient in  $[\text{O I}]/[\text{O III}]$  which is almost independent of abundance effects (see Ferland & Netzer 1983).

### 3.9.3. Density Gradient Effects

Considering the nucleus as the ionization source with an ionizing luminosity  $L_{\text{ion}}$ , the excitation conditions are governed by the ionization parameter:

$$U \propto L_{\text{ion}} r^{-2} N_e^{-1}. \quad (6)$$

If the radial dependence of the density is given by  $N_e \propto r^{-\beta}$ , then for  $\beta > 2$  one can get an increase in the excitation conditions as a function of radius. In fact, as shown in § 3.6.1, we measured a radial dependence of density with  $\beta \approx 0.6$  for the first  $5''$  around the nucleus. Considering the small range of density, our spatial resolution constraints, and the uncertainties involved in the measurements, this value must be considered a lower limit and therefore could still be consistent with the requirement  $\beta > 2$ ; however at face value this does not seem likely.

### 3.9.4. Local Ionizing Source

If the density within the emission region decreases outwards like  $r^{-2}$  or steeper as required to increase the ionization parameter with radius, and since the emissivity of the lines goes as  $N_e^2$ , we would naively expect the surface brightness of the emission line regions to go as  $F(\text{line}) \propto r^{-4}$  if the regions are ionized by the central nonthermal source located in the nucleus. In fact we measure  $F([\text{O III}] \lambda 5007) \propto r^{-2.35}$  and  $F(\text{H}\alpha) \propto r^{-2.50}$ , (see Figs. 11a and 11b). A similar behavior has been detected in the extended emission line regions around

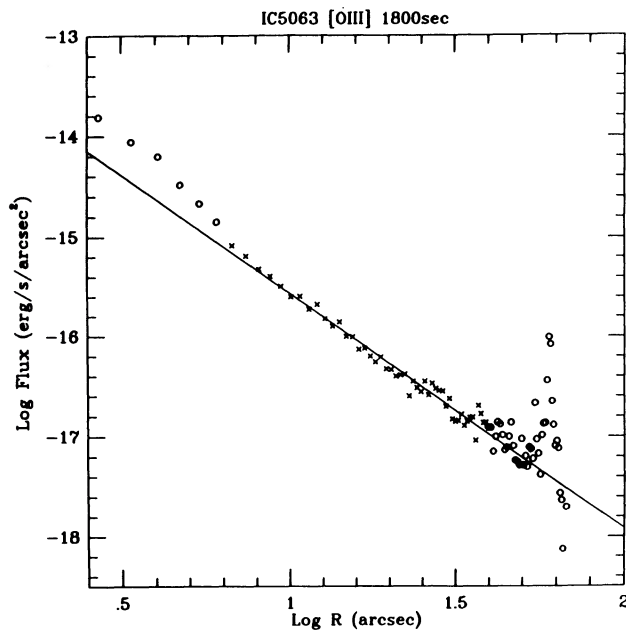


FIG. 11a

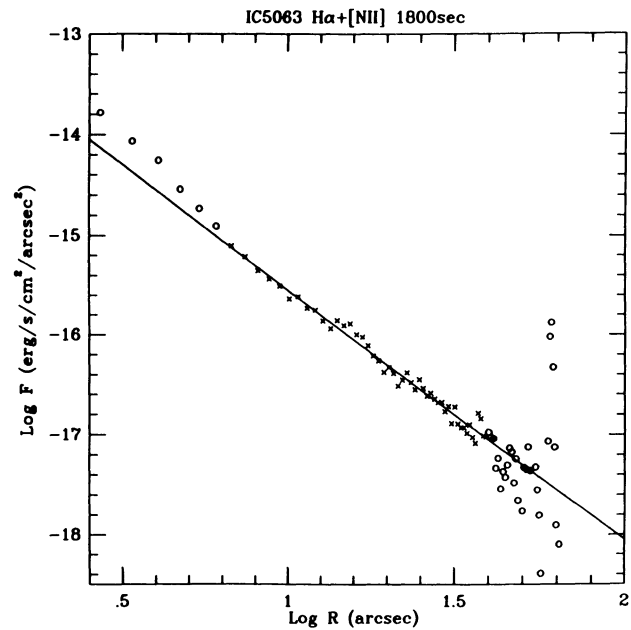


FIG. 11b

FIG. 11.—(a) Surface brightness of the  $[\text{O III}]$  emission-line regions as a function of distance. Also plotted is a linear fit with slope of  $-2.354$  and zero point of  $-13.208$ . (b) Surface brightness of  $\text{H}\alpha$  emission as a function of distance from the nucleus. The linear fit has slope of  $-2.5$  and zero point of  $-13.045$ .

3C 227 where the brightest regions are also those with the highest ionization parameter (Fosbury 1989).

Therefore to reconcile the increase of the ionization parameter and decrease of emission-line surface brightness, it may be necessary to invoke a local ionizing source, for example associated with a starburst or with the radio jet.

The extra ionizing photon flux is unlikely to be provided by a starburst, since the emission-line ratios indicate overall excitation conditions higher than expected from hot stars. Also, the ionization produced by relativistic electrons is very small compared with the ionization generated by a powerful active nucleus (Ferland & Mushotzky 1984; Wilson, Ward, & Haniff 1988).

An alternative to local ionization however, is that geometrical and environmental effects influence the *surface brightness* with radius. If the emitting material comprises discrete "clouds," the emission per cloud will be approximately  $\propto n_e^2 r_c^3$ . Hence, even if a given line of sight (per unit area) intercepts a fixed number of clouds, the resulting surface brightness will be  $F \propto n_e^2 r_c^2$ . For  $n_e \propto r^{-\beta}$  as above, and  $F \sim r^{-2.4}$  we need  $r_c \propto r^{(2\beta - 2.4)/3}$ .

### 3.9.5. Summary

We conclude that the combined effects of abundance and density gradients are the most likely reason for the positive excitation gradients in the ionized regions, with the radial variation of ionization parameter and surface brightness indicative of environmental modification to the emitting gas.

## 4. DISCUSSION

### 4.1. Origin of the Gas and Dust

Both the morphology of the dust/gas distribution and its kinematic properties support the idea of an external origin most likely due to a recent merger between an early-type elliptical or bulge-dominated S0 and a small gas-rich spiral. In the following, we review several arguments favoring this hypothesis.

1. As described in § 3.3.1, the dust extends over the whole optical image and has an unusual zig-zagging morphology roughly parallel to the IC 5063 optical major axis. This rather irregular appearance may arise as a consequence of warps within a plane of gas settling by differential precession into the principal plane of the underlying potential (Steiman-Cameron & Durisen 1990). The symmetry of the rotation curve suggests that the system is basically in rotation about the galaxy minor axis, although it may be that the unusual dust-lane morphology is related to the superposition of three distinct angular momentum vectors (two spin, or orbital) onto the dissipative gaseous medium. Also, although the innermost dust ring is symmetric in appearance, the inclination to the plane of the sky derived from its ellipticity (assuming it is circular) of  $75^\circ$  is significantly higher than the inclination of the emission-line disk (closer to the nucleus) as derived by DGW from kinematic considerations. This suggests that although essentially a two-dimensional structure, there are important deviations from a planar distribution, perhaps warps or waves within the gas disk, and this in turn may be related to the reason why we see such an extensive region of high-excitation emission-line gas.

2. Further support for a merger scenario comes from the comparison of the stellar and gas kinematical properties. Although it is unclear whether the directions of the stellar and gaseous rotation axes are coincident, larger velocity *gradients* are present in the ionized gas (Appenzeller & Gaida 1981;

DGW; BDB). Also our detection (§ 3.4) of a kinematic feature at  $1''.5$  SE of the nucleus along P.A.  $289^\circ$  confirms the observation by Caldwell & Phillips (1981) of a second emission-line component at  $2''.5$  SE along P.A.  $300^\circ$  and supports the deduced presence of counter-rotating gas near the center of IC 5063 (Wagner & Appenzeller 1989). As the latter authors point out, the time scale for such counter-rotating gas to survive against a massive gas system having different dynamical properties is expected to be very short (of the order of one or two orbital periods; Steiman-Cameron & Durisen 1990). This therefore also reinforces the idea that we are witnessing a transient event such as the remains of a recent merger.

3. The extended emission-line regions have element under-abundances factor of 2.5–10 solar (see § 3.6 and BDB). This indicates that this gas has not been heavily processed and favours an external origin.

4. Wardle & Knapp (1986) have shown that the H I detection of DGW represents an *anomalously large* amount of neutral gas, characterized by a total mass  $M_{\text{HI}} = 2.45 \times 10^9 M_\odot$  and by a mass-to-luminosity ratio  $M_{\text{HI}}/L_B = 0.19$ . These values place IC 5063 in the upper envelope of the S0 galaxy distribution according these two parameters. Also the measured H I velocity width ( $\Delta V$ ) of  $629 \text{ km s}^{-1}$  is located in the upper envelope defined in the  $\Delta V - L_B$  plane for S0 galaxies. Such extreme values are also indicative of an independent, external origin for the gaseous component. If, as suggested by the infrared surface photometry, IC 5063 should really be classified as an elliptical galaxy, then these values are even more extreme.

A gas/dust-rich galaxy has therefore apparently merged with IC 5063. The unusual dust-lane morphology is evidence for a transient state, while the inner rotating emission-line gas could indicate the existence of gas already settled into the principal plane of IC 5063. The counter-rotating gas within the very central regions could be associated with the core of the gas-rich galaxy that has survived the merging process (Balcells & Quinn 1990).

### 4.2. Hidden Luminous Active Nucleus

There are several lines of evidence suggesting the presence of a very powerful nonthermal source hidden in the nucleus of IC 5063. Here we discuss first the detection of high-excitation "coronal" emission lines, second, a very broad, faint H $\alpha$  emission line underlying the narrower nuclear emission, and third, the morphology of the high-excitation emission which assumes a well-defined "conelike" appearance. This leads to a discussion of the energetic balance between all components.

#### 4.2.1. Coronal Lines

We detect high-excitation emission lines like [Fe VII]  $\lambda\lambda 5721, 6087$  (ionization potential  $\text{Fe}^{6+} = 100 \text{ eV}$ ) and, less clearly, [Ca V]  $\lambda 5309$  (ionization potential  $\text{Ca}^{4+} = 67 \text{ eV}$ ) and [Fe X]  $\lambda 6375$  (ionization potential  $\text{Fe}^{9+} = 235 \text{ eV}$ ). These lines are seen only within the  $1''.5$  of the nucleus (see Fig. 12a and 12b), indicating therefore the presence of a local and hard extreme ultraviolet ionizing (HEUV) source. These lines can be produced either by collisional ionization in a dense cloud of hot gas ( $T_e \approx 10^6 \text{ K}$ ) or by photoionization by an HEUV non-thermal source. In the latter case the electron temperature would be of the order of  $10^4 - 5 \times 10^4 \text{ K}$ .

The physical conditions (density and temperature) in these very high-excitation regions can be obtained from the [Fe VII]  $\lambda 5159$ /[Fe VII]  $\lambda 6087$  and [Fe VII]  $\lambda 3759$ /[Fe VII]  $\lambda 6087$  line

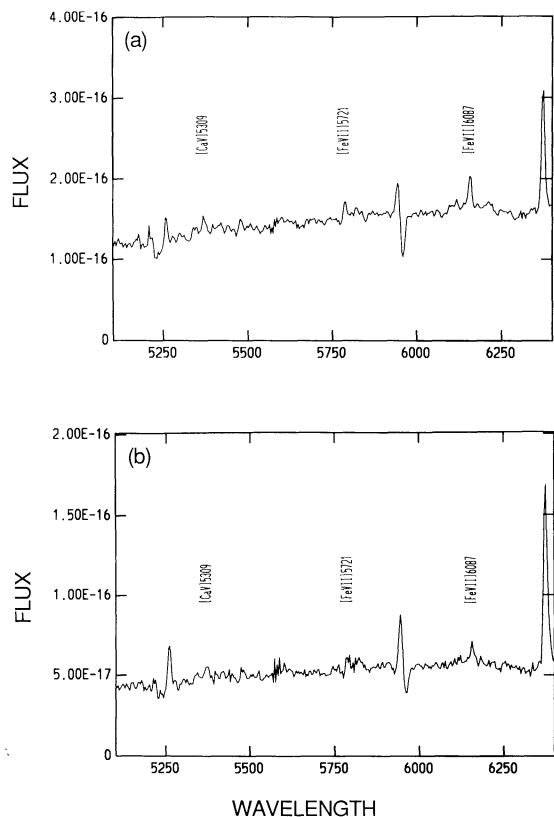


FIG. 12.—(a) Observed emission-line spectrum of the IC 5063 nucleus showing the high-excitation lines [Ca v]  $\lambda 5309$ , and [Fe VII]  $\lambda \lambda 5721$ , 6087. (b) Observed emission line spectrum at 2'' SE of the nucleus along P.A. 289°.

ratios, respectively (Nussbaumer & Storey 1982). Although extinction effects could play a rôle in decreasing the [Fe VII]  $\lambda \lambda 3759$ , 5159 line flux relative to the [Fe VII]  $\lambda 6087$  line, the fact that we do not detect any of these lines above the continuum can be considered as evidence of low ratios. This indicates densities and temperatures well below  $10^8 \text{ cm}^{-3}$  and  $10^5 \text{ K}$  since otherwise [Fe VII]  $\lambda 3759$ /[Fe VII]  $\lambda 6087 \approx 1.5$  and [Fe VII]  $\lambda 5159$ /[Fe VII]  $\lambda 6087 \approx 0.35$ .

In other Seyfert galaxies where these lines have been detected (for instance Tol 0109–383: Fosbury & Sansom 1983; IIZw77: Osterbrock 1981), the temperatures were also consistent with photoionization. Also the correlation between the luminosity in these lines and the lines of [O III]  $\lambda 5007$  and  $H\beta$  (Penston et al. 1984) reinforces the idea that these coronal lines are produced in general by photoionization.

We can estimate the number of ionizing photons with energy  $h\nu \geq 100 \text{ eV}$  needed to get the observed [Fe VII]  $\lambda 6087$  luminosity. If  $T_e(\text{Fe}^{6+}) = T_e(\text{O}^{++}) = 1.5 \times 10^4 \text{ K}$  and  $N_e(\text{Fe}^{6+}) \approx 10^7 \text{ cm}^{-3}$  we have

$$N_{\text{ph}}(h\nu > 100 \text{ eV}) \geq N(\text{Fe}^{6+})V \\ = L([\text{Fe VII}] \lambda 6087)[N(^1D)A(\lambda 6087)h\nu]^{-1} \quad (7)$$

where  $N(^1D) = N(\text{Fe}^{6+} \ ^1D_2)/N(\text{Fe}^{6+}) = 1.14 \times 10^{-2}$  for the appropriate (above) physical conditions (Nussbaumer & Storey 1982). Hence  $N_{\text{ph}}(h\nu > 100 \text{ eV}) \geq 2.4 \times 10^{51}$  photons  $\text{s}^{-1}$ . This lower limit lies well above the power-law extrapolation with index  $\alpha = 1.5$  of the observed UV flux ( $N_{\text{ph}}(h\nu > 100 \text{ eV}) \approx 2.72 \times 10^{49}$  photons  $\text{s}^{-1}$ ).

#### 4.2.2. Broad $H\alpha$ Emission Line

We clearly detect a faint, broad  $H\alpha$  emission line. This component is only seen within 1'' of the nucleus (see Figs. 13a and 13b) and its FWZI corresponds to a velocity of  $6000 \text{ km s}^{-1}$ . This is consistent with the claim of BDB that a broad  $H\alpha$  component with FWHM equal  $3200 \pm 500 \text{ km s}^{-1}$  is present. This faint, broad emission component could come from an obscured broad-line region whose radiation is scattered into our line of sight, following Antonucci & Miller (1985), or it may be a luminous nucleus seen directly but severely attenuated by a compact nuclear dust cloud.

#### 4.2.3. Ionization Cone

Figure 14 (Plate 5) shows an image of the ratio of [O III]/ $H\alpha$ , emphasizing the area of high excitation, and Figures 15a and 15b (Plates 6 and 7) color-codes the excitation in order to see the complete range. The excitation map has an overall X-morphology with a projected opening angle of  $50^\circ$  and sharp well-defined edges outside of which the emission is dominated by  $H\alpha$  radiation. It probably represents one of the best examples of a "cone" of high-excitation emission known to date. The dust and (presumably) cooler gas, on the other hand, are present throughout the galaxy, and therefore, since these are the most probable source for line-emitting material, this immediately suggests that different regions of the galaxy are seeing quite different radiation fields, which we quantify below. We propose therefore that we are observing a disk of gas in the plane of the galaxy illuminated in regions where it intersects a

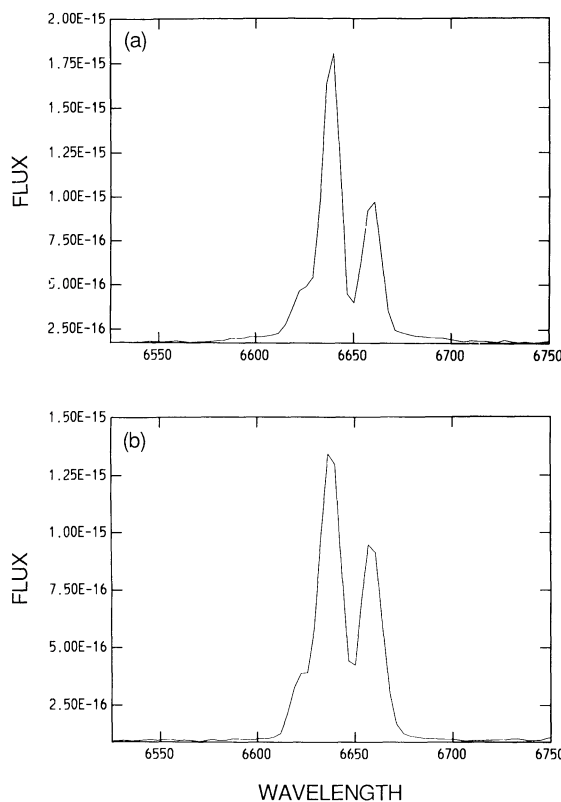


FIG. 13.—(a) Profile of the  $H\alpha$  emission line centered on the nucleus. The faint, broad emission-line component with FWZI equal to  $6000 \text{ km s}^{-1}$  is clearly visible. (b) Same emission-line profile, but centered at 1.4'' SE of the nucleus along P.A. 289°. Note that the broad, faint  $H\alpha$  component is no longer present.

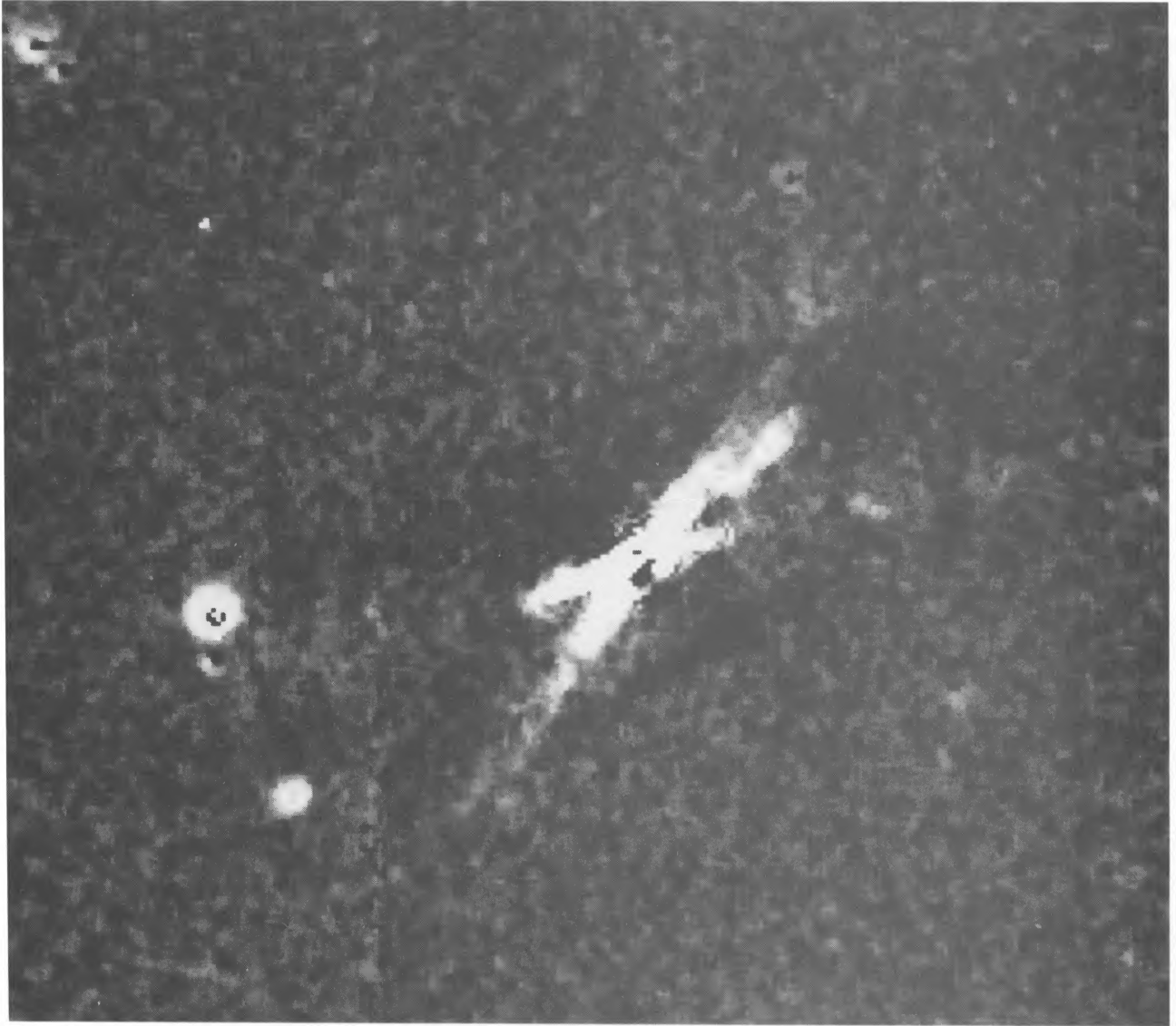


FIG. 14.—The  $[\text{O III}]/\text{H}\alpha$  excitation map showing the well-defined ionization cone with an opening angle ( $2\theta$ ) of around  $50^\circ$ . The gray scale is chosen to show high excitation as white and emphasises the X-morphology. The field of view is  $169'' \times 155''$ .

COLINA, SPARKS, & MACCHETTO (see 370, 113)

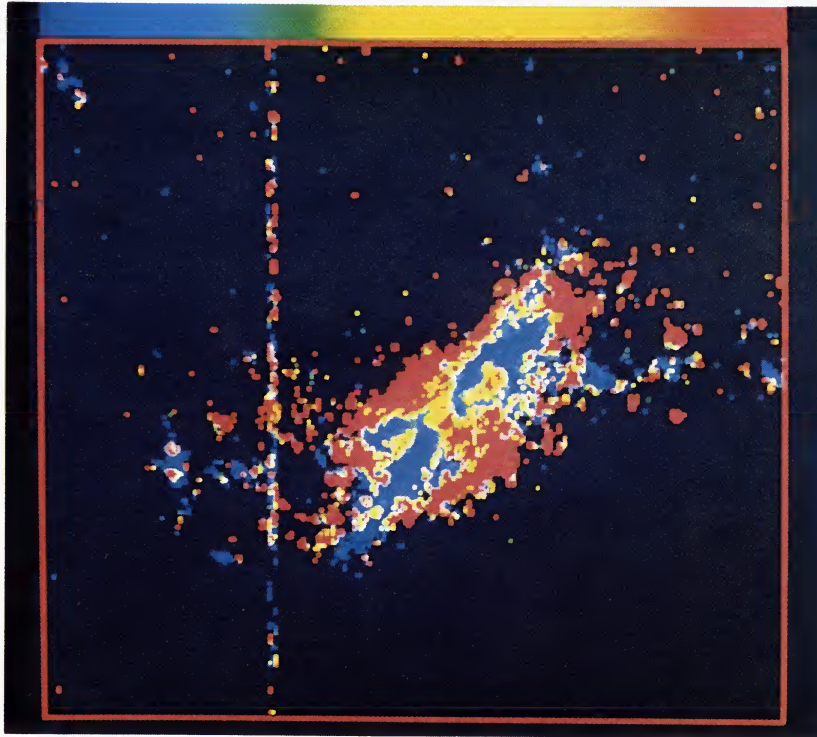


FIG. 15.—(a) Color-coded excitation map showing the full range of excitation conditions

COLINA, SPARKS, & MACCHETTO (see 370, 113)

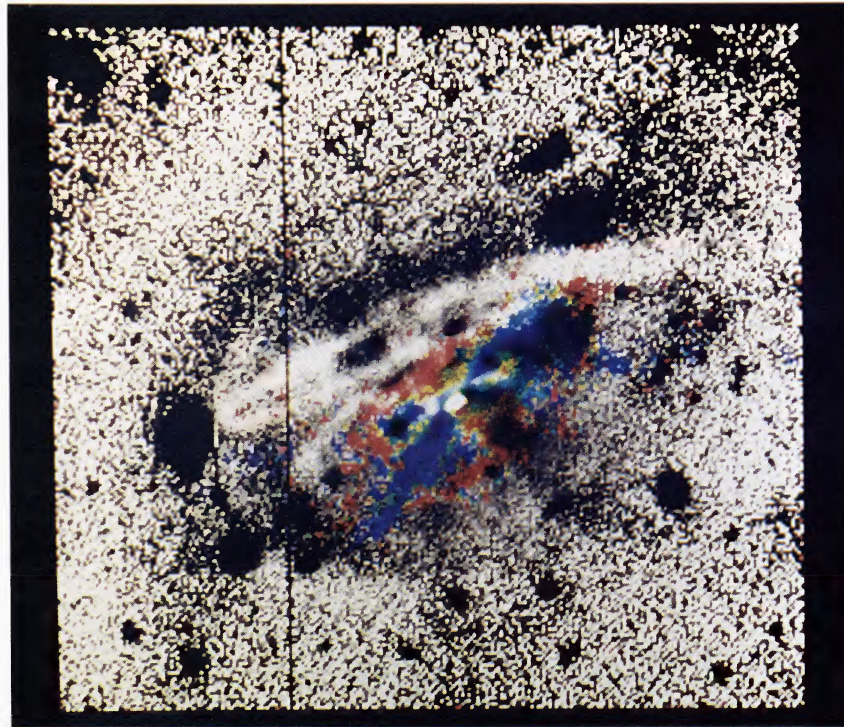


FIG. 15.—(b) Combination of the excitation map (Figs. 14 and 15a) color-coded onto the dust image (Fig. 5)

COLINA, SPARKS, & MACCHETTO (see 370, 113)

cone of ionizing radiation directed along the radio axis (to the west, out of the plane). In addition, the detailed structure of the high-excitation emission cone appears to be modulated by observable dust features, seen in Figure 15*b* and discussed in § 4.3, which may imply externally induced anisotropy rather than, or in addition to, intrinsically anisotropic nuclear radiation.

For a gas disc inclined at  $55^\circ$  to the plane of the sky lying in the plane of the galaxy to intersect a cone whose vertex points along the radio/polarization axis at  $\approx 90^\circ$ , such that the projected opening angle is  $50^\circ$ , the intrinsic cone opening angle must be  $\approx 100^\circ$ , and the cone axis must lie about  $30^\circ$  from the plane of the sky.

Although subject to assumptions about the spectrum of the ionizing radiation, further support for a hidden luminous nucleus comes from a direct comparison between the number of ionizing photons arriving at the extended emission-line regions and the number of ionizing photons along our line of sight. As described in § 3.8, the main emission-line ratios are consistent with an ionization parameter  $U \approx 7.5 \times 10^{-4}$  if a blackbody ionization source is appropriate, or  $U \approx 1.5 \times 10^{-2}$  if an  $\alpha = 1.5$  power-law source applies ( $F_\nu \propto \nu^{-\alpha}$ ).

Assuming a mean radius  $r$  equal to 1.3 kpc, and a mean electron density  $N_e$  equal to  $200 \text{ cm}^{-3}$ , the number of ionizing photons in a certain direction arriving at the extended emission-line regions, if a power-law spectral shape is assumed, is given by

$$N_{\text{ph}}(\text{EELR}) = Ur^2 N_e c, \quad (8)$$

and therefore the number of ionizing photons arriving at the extended emission-line regions is  $\log N_{\text{ph}}(\text{EELR}) = 54.2$  in units of photons  $\text{s}^{-1} \text{sr}^{-1}$  or  $\log N_{\text{ph}}(\text{total}) = 55.30$  photons  $\text{s}^{-1}$  for an isotropic source. For a hot blackbody the corresponding numbers are 52.9 and 54.0. These values are consistent with the number of ionizing photons obtained directly from the  $\text{H}\alpha$  luminosity:

$$N_{\text{ph}} = 7.52 \times 10^{11} L(\text{H}\alpha) \Omega^{-1} \text{ photons s}^{-1}, \quad (9)$$

where  $L(\text{H}\alpha)$  is in  $\text{ergs s}^{-1}$ ,  $\Omega$  is the covering factor of the emission-line regions (i.e., the fraction of incident photons intercepted) and case B recombination has been assumed (see Aller 1984). We found  $\log L(\text{H}\alpha) = 41.52 \text{ ergs s}^{-1}$  (see (§ 3.7), hence

$$N_{\text{ph}} = 2.49 \times 10^{53} \Omega^{-1} \text{ photons s}^{-1}, \quad (10)$$

so for typical covering factors  $\Omega$  between  $10^{-1}$  and  $10^{-2}$ , this gives  $N_{\text{ph}} \approx 2.5 \times 10^{54} - 2.5 \times 10^{55}$  photons  $\text{s}^{-1}$ .

On the other hand, if we extrapolate the measured UV flux [ $F_\nu(\lambda 1500) = 2.74 \times 10^{-28} \text{ ergs s}^{-1} \text{ cm}^{-2} \text{ Hz}^{-1}$  obtained from the Fig. 1*f* of Boisson & Durret 1986] into frequencies beyond the Lyman limit with the same power-law as before ( $\alpha = 1.5$ ), we have the number of ionizing photons coming towards us:

$$N_{\text{ph}}(\text{LOS}) = D^2 F_\nu(912 \text{ \AA})(\text{H}\alpha)^{-1}, \quad (11)$$

where  $D$  is 66 Mpc. This gives a value for the number of photons along our line of sight  $\log N_{\text{ph}}(\text{LOS}) = 50.74$  (in units of photons  $\text{s}^{-1} \text{sr}^{-1}$ ) which is *three orders of magnitude* smaller than the one measured in the emission-line regions (see following discussion in § 4.3). This large discrepancy cannot be removed by considering a flatter power-law spectrum (a slope as flat as 0.5 will increase the number of photons along our line of sight by a factor of 5). Carrying through a similar calculation for the blackbody parameters still results in one order of mag-

nitude too few photons from the extrapolated UV continuum, even if *all* the  $1500 \text{ \AA}$  flux came from the blackbody, which itself is inconsistent with the UV spectral shape and so must be considered an upper limit. It appears therefore that the gas within the galaxy "sees" more UV photons than we do at the present time.

#### 4.2.4. Infrared Properties

The galaxy IC 5063 is a powerful *IRAS* far-infrared source, with flux peaking at  $60 \mu\text{m}$ , and  $\log L_{\text{FIR}}(L_\odot) = 10.53$  (Heckman et al. 1989). When discussing possible origins for anisotropy, we show in the next section that this infrared emission is consistent with absorption and subsequent reradiation of an isotropic radiation field by dust. A possible problem for such an interpretation, but nevertheless an observation which supports the "hidden nucleus" argument is the high-infrared polarization measured by Hough et al. (1987) together with its very steep infrared spectral index (Axon et al. 1982; this paper, § 3.9). These authors suggested that IC 5063 contains a blazar-type nucleus whose magnetic field is aligned with the radio jet as in M87 and whose near-infrared radiation is nonthermal synchrotron emission. On the other hand, we found no evidence for variability which may argue against the blazar scenario. Difficulties with interpretation as hot dust are discussed in those papers.

#### 4.2.5. Variability Versus Anisotropy

All the above points indicate that the gas within IC 5063 is immersed in a radiation field quite different to that seen along our line of sight. This may arise either through spatial anisotropies (internally or externally induced) or else through time variations of the nuclear spectrum, so that at present the ionizing photons from the nucleus are reduced with respect to their average over the last few  $10^4 \text{ yr}$  (the light crossing time over the emission region). We found no direct evidence for short time scale variability (see previous section). More compelling, perhaps, is the overall morphology of the emission-line excitation distribution. The clear X-shaped pattern implies strong azimuthal variations of excitation conditions with no evidence for tangential structure that should arise from slower time variations. Given a clear observed azimuthal modulation of the radiation field, our natural choice between spatial or temporal variation of the ionizing spectrum is spatial—i.e., anisotropy rather than variability. Subsequent discussion continues on the assumption that we are not seeing strong time variability and that the nucleus as seen from the line-emitting regions is significantly more powerful than viewed along our own line of sight.

To summarize § 4.2 therefore, the presence of the coronal lines, indicating the existence of clouds with electron densities around  $10^6 - 10^7 \text{ cm}^{-3}$  or larger, being photoionized by an HEUV source and the faint broad  $\text{H}\alpha$  line are evidence for the presence of an obscured Seyfert 1 type source located in the nucleus of IC 5063. Along with the photon budget and infrared properties, these characteristics make the IC 5063 nucleus a good candidate for a high-luminosity active nucleus in which obscuration/orientation/beaming effects are playing an important rôle in diminishing its apparent luminosity. In § 4.3 we discuss these possibilities.

#### 4.3. Origin of the Anisotropy of the Central Ionizing Source

There is good evidence that IC 5063 contains a hidden luminous active nucleus and that the radiation field is anisotropic (§ 4.2). Several different mechanisms for this phenome-

non have been proposed, including anisotropic radiation from an accretion disc, selective obscuration due to dust extinction or relativistic beaming (see Browne 1989 for a review). In low-luminosity active galaxies there is so far no evidence of relativistic motions, while the morphology of the extended emission-line regions around these galaxies indicates the existence of a wide ionizing source. This constraint is difficult to account for within the beaming hypothesis since any source with a large Lorentz factor is likely to be highly collimated and any change in its direction of motion would generate drastic variations in the observed brightness of the source. We therefore discuss in detail two alternatives that may explain the anisotropy either separately or in combination.

#### 4.3.1. Accretion Disk Radiation

As shown in § 3.8, the ratios of the main emission lines are consistent with a  $1.3 \times 10^5$  K blackbody radiation field and ionization parameter  $U = 7.5 \times 10^{-4}$ . This temperature is consistent with the effective temperature of the inner parts ( $R \leq 410R_g$  where  $R_g = 2GM_{\text{BH}}c^{-2}$ ) of an optically thick, geometrically thin radiation torus around a massive blackhole (Madau 1988).

In this case the discrepancy between the number of photons arriving at the EELR and along our line of sight is decreased. On one hand, the blackbody radiation produces a larger fraction of photons, by a factor of 20 with respect to a power-law slope, capable of ionizing  $\text{O}^{++}$ , i.e.,  $N_{\text{ph}}(\text{EELR})$  decreases. On the other hand, given a certain level in the observed UV flux, there are more photons around the Lyman limit for a blackbody type radiation than for power-law type radiation, i.e.,  $N_{\text{ph}}(\text{LOS})$  would be increased.

Also, Madau's model of the radiation field of an optically thick, geometrically thin accretion disk predicts uniform ionization conditions over an opening angle of around  $60^\circ$ , while the flux of UV and X-ray photons will drop dramatically outside this region. This is due to scattering effects produced in the inner walls of the accretion disk which act as a mirror. This scattering will concentrate most of the ionizing photons within the  $60^\circ$  cone producing an enhancement (beaming) of the ionizing luminosity in these extended emission-line regions. This kind of behavior is similar to the morphology of the high-excitation emission in IC 5063: we find similar ionization conditions within the cone and a sharp edge; outside this cone, no indications of high-excitation conditions are present.

#### 4.3.2. Selective Directional Extinction

The  $[\text{O III}]/\text{H}\alpha$  excitation map, Figures 14 and 15a, shows a wide high-excitation cone with an opening angle of  $50^\circ$  in projection. This structure is similar to those recently detected in other nearby Seyfert galaxies like NGC 1068 (Pogge 1988a), NGC 4388 (Pogge 1988b), NGC 5252 (Tadhunter & Tsvetunov 1989), and NGC 4151 (Pérez et al. 1989; Pérez-Fournon & Wilson 1990).

In IC 5063 we find that only low-excitation gas is present in directions perpendicular to the high-excitation cone, suggesting therefore that there is a lack of highly energetic ionizing photons along these directions. This shadowing could be due to the presence of obscuring material near the nucleus. In the determination of the number of ionizing photons arriving along our line of sight, we did not enter any extinction correction due to internal dust lying between us and the central source. Based on the UV and optical continuum shape, Boisson & Durret (1986) derived an extinction  $E(B-V) = 0.12$ , while our  $\text{H}\beta/\text{H}\gamma$  ratio gives an upper limit

$E(B-V) = 0.40$  for the observed emission from the nuclear region. Extinction measured from our dust image also gives values  $E(B-V)$  around 0.1–0.2 typically. Since  $A(912 \text{ \AA}) \approx 20E(B-V)$ , the  $N_{\text{ph}}(\text{LOS})$  could be increased by a factor of as much as 1000. This could explain, at least in luminosity, the discrepancy between the number of photons arriving to the emission-line regions and along our line of sight if the emission regions themselves have an *unobscured* view of the nucleus.

In addition, the influence of obscuring material is clearly visible when comparing our optical depth image (Fig. 4b) with the excitation map (Figs. 14 and 15a). The ring of dust around the nucleus fits neatly into the gap in the excitation cone observed at P.A.  $300^\circ$ , and structure in both the NW and SE dust regions is correlated with excitation conditions, strongly suggestive of direct modification of the radiation field by absorbing material. Figure 15b attempts to show this behavior by color-coding the excitation conditions onto an image of the dust optical depth.

The existence of obscuring material could also be favoured by the large *IRAS* infrared luminosities measured in this galaxy. The total FIR luminosity corresponds to  $\log L_{\text{FIR}}(L_\odot) = 10.53$ . According to Rowan-Robinson & Crawford (1989), a dust mass  $M_D = 1.07 \times 10^3 M_\odot$ , and distances between 1–100 pc from the nucleus are required to explain the *IRAS* flux if dust particles are heated by the central non-thermal source.

Now, returning to the photon budget arguments of § 4.2.3, where we found that the number of ionizing photons per second (assuming isotropy) for a power law and for a hot blackbody were  $2 \times 10^{55}$  and  $1 \times 10^{54}$ , respectively, we can deduce corresponding UV luminosities by multiplying by the mean photon energy. This gives for the power law assumption  $L_{\text{UV}} \approx 2 \times 10^{45}$  ergs  $\text{s}^{-1}$ —extremely large and rather implausible. The blackbody assumption gives  $L_{\text{UV}} \approx 6 \times 10^{43}$  ergs  $\text{s}^{-1}$ . The two numbers bracket well the observed infrared emission which, if due to re-radiated UV radiation, should be  $L_{\text{IR}} \approx \Omega_d L_{\text{UV}}$  where  $\Omega_d$  is the dust covering factor—64% if the outer cone edge is due to an inner minor axis dust ring obscuring the nucleus for the cone parameters given above. Clearly with relatively minor modification to the blackbody spectrum, it should be possible to bring these luminosities into agreement, and we conclude that the data are consistent with the infrared emission coming from dust reradiation of a substantial fraction of the emitted UV continuum.

In conclusion we believe that because of morphological and energetic considerations, the radiation anisotropy observed in IC 5063 is most likely due primarily to obscuring material outside but close to the central source, although the intrinsic accretion disk radiation field cannot be excluded.

## 5. SUMMARY AND CONCLUSIONS

The results obtained using new deep-IR, optical images and long-slit spectroscopy of IC 5063 and its associated extended emission-line regions can be summarized as follows:

1. We map clearly for the first time the system of zig-zagging dust lanes over the whole northern half of the galaxy, running approximately parallel to the major optical axis and seen all the way down to the nucleus. We also map the extended emission-line regions concentrated along the major axis of the galaxy and having a total extent in projection of  $22 \times 6.4$  kpc.
2. We measure a velocity field in the ionized gas which is consistent with a rotational disk with major axis along P.A.

300°. We also detect a counter-rotation or radial flow feature in the velocity field at 1'5 SE of the nucleus at P.A. 289°.

3. We measure ionized gas element underabundances of a factor of 3. The electron temperature is  $1.5 \times 10^4$  K in the inner 1.5 kpc and the electron densities are in the 100–500  $\text{cm}^{-3}$  range. The density has a negative radial gradient consistent with a slope of 1, although steeper gradients can be present. The reddening within these emission-line regions is in the range  $E(B-V) = 0.1-0.40$ .

4. The total amount of ionized gas in the extended emission-line regions is in the range  $M_T(\text{gas}) \geq 5 \times 10^6 M_\odot$ , while the filling factor is  $f = 10^{-4}$ . This compares with  $M(\text{H I}) = 4 \times 10^8 M_\odot$  from the dust observations and  $1 \times 10^9 M_\odot$  from the H I radio measurement.

5. The mean excitation conditions within the extended emission-line regions are consistent with an ionization parameter  $U = 7.5 \times 10^{-4}$  and a  $1.3 \times 10^5$  K blackbody radiation. They are also consistent with an ionization parameter  $U = 1.5 \times 10^{-2}$  and a nonthermal power law with  $\alpha = 1.5$ ; however, that imposes difficulties for the overall energy budget.

6. We detect positive excitation gradients outwards from the nucleus which can be explained as the combined effect of negative density and abundance gradients.

7. We measure a surface brightness decrease in the emission-line regions flatter (slope  $\approx 2.5$ ) than expected if the electron density decreases with a slope  $\geq 2$  and emission measure variations arise solely from density changes. This can be understood as evidence for environmental and geometric effects influencing the emission measure through cloud size or path length variations (see also point 6 above).

8. We detect a cone of high-excitation gas along P.A. 300° and opening angle of 50°. Within this, excitation conditions are roughly uniform, while outside, excitation conditions drop very rapidly. The ionizing radiation flux as derived from the

emission-line radiation within this cone is a factor of  $10^3$  larger than along our line of sight if a power-law UV spectrum is present, and similar imbalances occur for a blackbody UV spectrum.

9. Dust effects are clearly present within the extended emission-line regions as indicated by a correlation between the presence of dust lanes and a decrease in excitation conditions within the cone. The FIR luminosity is consistent with dust reradiation of the bulk of the UV emission whose spectrum should be quite close to a blackbody, as inferred from comparison with spectral models.

10. We detect high-excitation [Fe VII] and [Ca V] emission lines and a broad, faint H $\alpha$  emission-line component (FWZI  $\approx 6000 \text{ km s}^{-1}$ ) around the first 1"–1'5 of the nucleus.

These individual points taken together lead us to the following simplifying propositions:

The system of gas and dust with the peculiar morphology, kinematics and low element abundance has most likely an external origin and can be considered as the remnant of a recent merger.

The extended emission-line regions are ionized by a central source located at the nucleus of IC 5063. This source has an ionizing luminosity of the order of  $10^{44} \text{ ergs s}^{-1}$  which places it at the level of luminous Seyfert 1 galaxies. The radiation field is compatible with an anisotropic source radiating with a projected opening angle of 50° and intrinsic opening angle of almost 100°. This anisotropy is consistent with obscuration, although intrinsic anisotropic radiation from a thick accretion disk cannot be discarded.

The authors wish to thank Dan Golombek for his assistance with the reduction of the data. Luis Colina wishes to acknowledge the support of an ESA postdoctoral fellowship during the course of this work.

#### REFERENCES

- Aller, L. H. 1984, *Physics of Thermal Gaseous Nebulae* (Dordrecht: Reidel)
- Antonucci, R. R. J. 1990, *Proc. 14th Texas Symposium on Relativistic Astrophysics*, in press
- Antonucci, R. R. J., & Miller, J. S. 1985, *ApJ*, 297, 621
- Appenzeller, I., & Gaida, G. 1981, *A&A*, 102, 230
- Axon, D. J., Bailey, J., & Hough, J. H. 1982, *Nature*, 299, 234
- Balcells, M., & Quinn, P. 1990, *ApJ*, 361, 381
- Barthel, P. D. 1989, *ApJ*, 336, 606
- Baum, S. A., Heckman, T. M., Bridle, A., van Breugel, W., & Miley, G. 1988, *ApJS*, 68, 526
- Bergeron, J., Durret, F., & Boksenberg, A. 1983, *A&A*, 127, 322 (BDB)
- Boisson, C., & Durret, F. 1986, *A&A*, 168, 32
- Browne, I. W. A. 1989, *ESO Workshop on Extranuclear Activity in Galaxies*, ed. E. J. A. Meurs & R. A. E. Fosbury (Munich: ESO), 379
- Bushouse, H. A. 1987, *ApJ*, 320, 49
- Byrd, G. G., Sundelius, B., & Valtonen, M. J. 1987, *A&A*, 171, 16
- Byrd, G. G., Valtonen, M. J., Sundelius, B., & Valtaoja, L. 1986, *A&A*, 166, 75
- Caldwell, N., & Phillips, M. M. 1981, *ApJ*, 244, 447
- Chambers, K. C., & Miley, G. K. 1990, *Proc. Hubble Centennial Symposium*, in press
- Chambers, K. C., Miley, G. K., & van Breugel, W. 1987, *Nature*, 329, 604
- Colina, L., Fricke, K. J., Kollatschny, W., & Perryman, M. A. C. 1987, *A&A*, 178, 51
- Colina, L., & Pérez-Fournon, I. 1990, *ApJS*, 72, 41
- . 1990b, *ApJ*, 348, 45
- Colina, L., Sparks, W., & Macchetto, F. D. 1990, *Proc. Conf. Paired and Interacting Galaxies*, ed. J. W. Sulentic, W. Keel, & C. M. Telesco (NASA CR 3098), p. 451
- Dahari, O. 1984, *AJ*, 89, 966
- Danziger, I. J., Goss, W. M., & Wellington, K. J. 1981, *MNRAS*, 196, 845 (DGW)
- Ferland, G. J., & Mushotzky, R. F. 1984, *ApJ*, 286, 42
- Ferland, G. J., & Netzer, H. 1983, *ApJ*, 264, 105
- Ferland, G. J., & Osterbrock, D. E. 1985, *ApJ*, 289, 105
- . 1986, *ApJ*, 300, 658
- Fosbury, R. A. E. 1989, *ESO Workshop on Extranuclear Activity in Galaxies*, ed. E. J. A. Meurs & R. A. E. Fosbury (Munich: ESO), 169
- Fosbury, R. A. E., & Sansom, A. E. 1983, *MNRAS*, 204, 1231
- Fricke, K. J., & Kollatschny, W. 1989, *IAU Symp. 134, Proc. Conf. Active Galactic Nuclei*, ed. D. E. Osterbrock & J. S. Miller (Dordrecht: Reidel), 425
- Hansen, L., Nørgaard-Nielsen, H. U., & Jørgensen, H. E. 1987, *A&AS*, 71, 465
- Heckman, T. M., Blitz, L., Wilson, A., Armus, L., & Miley, G. 1989, *ApJ*, 342, 735
- Heckman, T. M., Smith, E. P., Baum, S. A., van Breugel, W., Miley, G. K., Illingworth, G. D., Bothun, G. D., & Balick, B. 1986, *ApJ*, 311, 526
- Hernquist, L. 1989, *Nature*, 340, 687
- Hough, J. H., Brindle, C., Axon, D. J., Bailey, J., & Sparks, W. B. 1987, *MNRAS*, 224, 1013
- Hutchings, J. B. 1987, *ApJ*, 320, 122
- Kennicutt, R. C., & Keel, W. C. 1984, *ApJ*, 279, L5
- Koski, A. T. 1978, *ApJ*, 223, 56
- Lin, D. N. C., Pringle, J. E., & Rees, M. J. 1988, *ApJ*, 328, 103
- Macchetto, F. D., Colina, L., Golombek, D., Perryman, M. A. C., & di Serego Alighieri, 1990, *ApJ*, in press
- Madau, P. 1988, *ApJ*, 327, 116
- MacKenty, J. W. 1989, *ApJ*, 343, 125
- McCarthy, P. J., van Breugel, W., Spinrad, H., & Djorgovski, S. 1987, *ApJ*, 321, L29
- Netzer, H. 1985, *MNRAS*, 216, 63
- . 1987, *MNRAS*, 225, 55
- Nussbaumer, H., & Storey, P. J. 1982, *A&A*, 113, 21
- Osterbrock, D. 1981, *ApJ*, 246, 696
- Penston, M. V., Fosbury, R. A. E., Boksenberg, A., Ward, M. J., & Wilson, A. S. 1984, *MNRAS*, 208, 347
- Pérez, E., Gonzalez-Delgado, R., Tadhunter, C., & Tsvetanov, Z. 1989, *MNRAS*, 241, 31p
- Pérez-Fournon, I., & Wilson, A. S. 1990, *ApJ*, 356, 456
- Pogge, R. W. 1988a, *ApJ*, 328, 519
- . 1988b, *ApJ*, 332, 702
- Robinson, A., Binette, L., Fosbury, R. A. E., & Tadhunter, C. N. 1987, *MNRAS*, 227, 97
- Rowan-Robinson, M., & Crawford, J. 1989, *MNRAS*, 238, 523
- Sanders, D. B., Soifer, B. T., Elias, J. H., Madore, B. F., Matthews, K., Neugebauer, G., & Scoville, N. Z. 1988, *ApJ*, 325, 74

- Smith, E. P., & Heckman, T. M. 1989, ApJ, 341, 658  
Sparks, W. B., Wall, J. V., Thorne, D., Jorden, P., van Breda, I. G., Rudd, P., & Jørgensen, H. E. 1985, MNRAS, 217, 87  
Steiman-Cameron, T. Y., & Durisen, R. H. 1990, ApJ, 357, 62  
Tadhunter, C. N., Fosbury, R. A. E., di Serego Alighieri, Bland, J., Danziger, I. J., Goss, W. M., McAdam, W. B., & Snijders, M. A. J. 1988, MNRAS, 235, 403  
Tadhunter, C. N., Fosbury, R. A. E., Binette, L., Danziger, I. J., & Robinson, A. 1987, Nature, 316, 733  
Tadhunter, C. N., Fosbury, R. A. E., & Quinn, P. J. 1989, MNRAS, 240, 225  
Tadhunter, C. N., & Tsvetanov, Z. 1989, Nature, 341, 422  
Ulvestad, J. S., & Wilson, A. S. 1984, ApJ, 285, 439  
Unger, S. W., Pedlar, A., Axon, D. J., Whittle, M., Meurs, E. J. A., & Ward, M. 1987, MNRAS, 228, 671  
Wagner, S., & Appenzeller, I. 1989, A&A, 225, L13  
Wardle, M., & Knapp, G. R. 1986, AJ, 91, 23  
Wilson, A. S., & Baldwin, J. A. 1989, AJ, 98, 2056  
Wilson, A. S., Ward, M. J., & Haniff, C. A. 1988, ApJ, 334, 121